Learning-related oscillatory dynamics in the human cortico-basal ganglia network during motor sequence initiation in Parkinson's Disease

Kara N. Presbrey, Thomas A. Wozny, Kenneth H. Louie, Simon Little, Philip A. Starr, Reza Abbasi-Asl*, Doris D. Wang*

ABSTRACT

Learning fine motor sequences is crucial to quality of life and can be altered in Parkinson's Disease (PD). It may be partially driven by the optimization of motor preparation and initiation, but neither pre-movement neural activity nor its optimization is well understood. One theory of general motor initiation posits that network beta (β) desynchronization releases motor cortical excitability, reflected as delta (δ) phase response, which in turn facilitates sequence-specific motor cortical ensemble activity to produce voluntary movement. With motor sequence learning, increases in cortico-basal ganglia δ synchrony may facilitate enhanced recruitment of both cortical and basal ganglia neural ensembles, increasing the reliability of their firing patterns. As gamma (γ) activity can correlate with spiking population dynamics, this model predicts learning-dependent pre-movement sequence-specific γ activity, alongside β→δ→γ interactions and cortico-basal ganglia δ phase synchrony—any of which could differ in PD. We test this model in four subjects with PD, on dopaminergic medication without deep brain stimulation, by leveraging invasive cortico-basal ganglia field potential recordings during a multi-day, multi-sequence typing task. Possibly indicative of PD-related neuropathophysiology, there was no consistent evidence for a full cascade of β→δ→γ gating of general motor initiation. However, subjects who improved with practice did demonstrate 1) practice-driven increases in the discriminability of sequence-specific γ activity and 2) cortico-basal ganglia δ synchrony that appeared to reflect a framework for learning-dependent δ-β and δ-γ coupling. In subjects who did not improve, discriminability of sequence-specific γ activity rather decreased with practice, and basal ganglia was functionally disconnected from cortex, instead dominated by ongoing subcortical δ oscillations. These findings suggest a model in which phase-responsiveness of basal ganglia δ to cortex is a predictor of motor learning.

INTRODUCTION

Fine motor control is a fundamental aspect of human motor function. Skilled hand movements must be learned, and proficiency is vital to maintaining individual autonomy and quality of life. Individuals with Parkinson's Disease (PD) can experience difficulty in fine motor skill learning and initiation[1,2], but the neural dynamics of motor learning remain poorly understood. We leverage invasive, mesoscale cortico-basal ganglia electrophysiology during a multi-day, multi-sequence typing task to evaluate the learning-dependent motor control network dynamics of motor initiation in individuals with PD.

Behavioral experiments suggest that, before the onset of rapid fine motor sequences like typing, humans can plan multiple sequence elements[3–7] and that learning involves the optimization of this sequence-specific process[3,4]. This may be facilitated neurophysiologically by the sequence-specific serial activation of neurons in motor cortical and basal ganglia (BG) ensembles, with motor improvement partly driven by the optimization of ensemble activity[8,9]. Indeed, sequence-specific pre-movement spiking activity has been observed in the primary motor cortex of nonhuman primates[10,11]. Moreover, the advanced activation of movement-specific motor cortical ensembles biases later action selection in rodents[12], and reduced variability in motor cortical and striatal spiking patterns around motor onset has repeatedly been shown to correlate with performance level and learning in rodents and nonhuman primates[13–17]. If these results translate to humans, gamma (γ) activity—a neural correlate of population spiking activity in mesoscale electrophysiology[8,18] that increases in amplitude with motor onset[8,19,20]—might reflect sequence-specific and learning-related ensemble activity in motor cortex and basal ganglia. However, though pathological changes in learning-related ensemble activity could contribute to a possible alteration of motor preparation in PD[21–23], this has never been investigated electrophysiologically. Thus, we first ask: Prior to the onset of movement, in which brain regions might mesoscale electrophysiological activity reflect sequence-specific neural dynamics in individuals with PD, and which electrophysiological properties of this activity are associated with performance improvement? We test this with single-trial classification and feature analysis of pre-movement neural activity.

We next evaluate how enhanced recruitment of pre-movement sequence-specific neural activity with learning may be supported by learning-driven changes in oscillatory network dynamics. Theories on the contributions of oscillatory network dynamics to the temporal unfolding of motor initiation often postulate the following cascade as instrumental in individuals without movement disorders. Network-wide beta (β) desynchronization[8,19,24,25] releases motor cortical excitability[21,26], reflected by delta (δ) phase response[8,13,27–31]. Excitability facilitates the activation of motor cortical ensembles to initiate movement[32,33], which correlates with increasing γ magnitude[18–20]. Work in animal models suggests that motor learning-related optimization of ensemble activity may result from increased coupling between δ and ensemble firing in striatum and motor cortex[8,13]. That this develops in conjunction with motor corticostriatal coordinated δ activity[34] ultimately poses coordinated δ activity as an ideal substrate for facilitating learning-related enhancements in neural ensemble recruitment. However, while the temporal cascade of changes in β, δ and γ activity has been repeatedly observed, neither the implied β→δ→γ gating interactions nor their relationship with cross-area coordinated δ activity have been rigorously tested with cortico-subcortical electrophysiology and directed connectivity analysis. Thus, we next analyze the learning stage dependence of directed δ-β and δ-γ coupling and δ phase synchrony.

In the course of our aforementioned approach, we finally aim to address a frequently overlooked issue in motor sequence learning studies: dissociation of the overlapping processes related to learning a motor sequence (sequence learning) from those related to acclimatization to a motor paradigm more generally (task learning). While sequence learning may, for example, involve improvements in motor sequence planning[3,4], task learning may involve optimization of task-related cognitive processes[35–40] and motor familiarization with the experimental apparatus[3]. As these learning processes could temporally overlap, the detection of sequence learning-related signals could be confounded by the parallel occurrence of task learning-related signals. To dissociate them, we employ a behavioral paradigm inspired by previous neuroimaging work[41] that aims to address this core issue.

Four individuals with PD had electrodes in either 1) striatum (Str), primary (M1) and premotor (PM) cortex or 2) subthalamic nucleus (STN), primary motor and parietal (Par) cortex (Figure 1A). All subjects were on dopaminergic medication and continuously off deep brain stimulation (DBS). In each subject group, one subject improved (improver), and the other did not (nonimprover). Pre-movement sequence-specific γ activity

occurred in all recorded brain regions (Figure 1B). In improvers, the discriminability of sequence-specific γ activity increased with practice in most brain regions; in M1, this was associated with increased δ→γ coupling. Improvers also displayed cortically-led motor network δ synchrony and various cross-frequency couplings (CFCs), reflecting the unique roles of different brain regions in sequence learning and with task exposure. In contrast, the discriminability of sequence-specific γ activity decreased in most brain regions in nonimprovers and was accompanied by high inter-basal ganglia δ coherence and minimal learning-related functional connectivity. Though all subjects showed M1 β desynchronization, δ phase response and γ synchronization, no subjects demonstrated a consistent β→δ→γ cascade—possibly indicative of PD-related neuropathophysiology. This work describes a learning-dependent hierarchical functional network architecture for complex manual skill initiation in PD and may inform the development of targeted neuromodulatory strategies for alleviating pathological neural dynamics.

RESULTS

Four individuals with PD receiving bidirectional neural interfaces for DBS were recruited for the study (Table 1, Figure 2). Bipolar recording of subcortical local field potentials (LFPs) and sensorimotor electrocorticography (ECoG) signal granted coverage of the following approximate regions. Subjects GP1 and GP2: globus pallidus (GP), putamen (Put), M1 or primary sensorimotor cortex (M1/S1), premotor cortex. Subjects STN1 and STN2: ventral subthalamic nucleus (vSTN), dorsal subthalamic nucleus (dSTN), M1, parietal cortex (spanning S1 and superior parietal lobule).

On each day of a multi-day explicit motor learning experiment, subjects practiced typing two five-element sequences in interleaved blocks using their dominant (right) hand while neural activity was recorded from the contralateral hemisphere (Figure 3A). After memorizing the sequences at the start of each session, subjects practiced the sequences from memory. In each training block, they practiced only one sequence, typing it once in response to each cue, as quickly and accurately as possible. The day before the experiment, subjects were familiarized with the task and keypad with a practice run-through (Familiarization). They received two novel sequences on Day 1 and again on Day 4 (Figure 3B, Table 2). All subjects performed the experiment within one month after DBS surgery, before turning on DBS. No DBS was delivered during or between experimental sessions. To limit the effect of medication-related motor fluctuations, we facilitated all experimental sessions at a consistent time point within a given individual's daily medication schedule.

Finger movements were detected using a custom-built keypad with capacitive proximity sensors and force-sensitive resistors on key switches, and visual stimuli were detected with a photodiode (Figure 3C). Neural alignment pulses were detected at the case of the implanted pulse generator. All behavioral sensors were sampled at 4 kHz with a custom-built motherboard for neural-behavioral data alignment. All neural analysis was performed on data from the reaction time (RT) period.

Behavioral stratification

To evaluate overall learning trends, we computed a block performance index for each subject (Figure 4, Figure 4—figure supplements 1 and 2). Each block performance index is the sum of block average error rate (1 – block accuracy), reaction time (cue presentation to movement initiation) and trial duration (movement onset to offset). Block average trial duration and reaction time were each first within-subject min-max scaled across days to [0,1]. Lower performance index values indicate better performance.

For behavioral stratification, sequence learning was assigned when there was both improvement from Day 1 to Day 3 and performance worsening from Day 3 to Day 4. A Day 1 to Day 4 comparison to assess task learning may be confounded by behavioral interference between the familiar sequences and those presented on Day 4, so we did not attempt to behaviorally stratify based on task learning.

GP1 and STN1 showed indications of sequence learning, whereas GP2 and STN2 did not. In GP1 and STN1, performance index improved for both sequences from Day 1 to Day 3, then worsened when practicing novel sequences on Day 4. Neither GP2 nor STN2 showed significant improvements in Sequence 1 (S1) and Sequence 2 (S2) performance index, and only GP2's performance index significantly differed between Days 3 and 4. These results suggest behavioral stratification as follows: improvers (GP1 and STN1) and nonimprovers (GP2 and STN2), with the qualification that GP2 showed signs of trending improvement.

Sleep durations and end-of-session upper limb MDS-UPDRS[42] scores were similar between groups (Table 3), suggesting relative differences in performance improvement may not have been due to large differences in sleep or motor symptom presentation in the typing arm.

Pre-movement sequence-specific γ activity is detectable throughout the recorded network and becomes increasingly predictive of sequence identity with performance improvement

To evaluate the involvement of different brain regions in sequence-specific initiation activity and how this involvement may change with learning, we performed single-trial classification of pre-movement neural activity and assessed changes in discriminability of sequence-specific activity across days. For each experiment day and for each recording channel per subject, we performed feature selection on neural data preceding sequential movement onset and trained a model to predict the identity of the sequence that the subject was about to type (Figure 5A–B, Figure 5—figure supplement 1). To isolate practice-driven changes in sequence-specific neural activity from changes that occur as a byproduct of the changing behavior, we only directly compared neural activity between sequences for which overall behavioral performance was similar. In most subjects, performance level significantly differed between Sequences 3 and 4 (Figure 5—figure supplement 2), so Day 4 data was excluded from single-trial classification analysis. To reduce the influence of neural activity related to the first sequence element, we designated the same digit as the first element in all sequences for each subject. See *Methods: Trial Selection* and *Methods: Single-Trial Classification* for additional measures taken to reduce the influence of confounds.

Sequence-specific pre-movement spiking activity has been detected in primate motor cortex[10,11], and learning enhances the reliability of motor cortical and striatal ensemble firing in rodents[17]. Thus, we predicted the presence of sequence-specific motor cortical and striatal activity that increases in predictive value with performance improvement. We compared each model's performance to chance and tested within-channel change in decoding accuracy across Days 1 and 3, with the caveat that Day 1 to Day 3 changes in decoding accuracy may reflect both sequence practice- and task exposure-related changes in neural activity. Notably, all models significantly outperformed chance (Figure 5C). Models trained on data from improvers showed broadly increasing decoding accuracy across days (GP, Put, M1/S1, PM, vSTN, dSTN, M1), whereas models for nonimprovers decreased across days instead in GP, STN and M1. These results suggest that pre-movement sequence-specific ensemble activity may have been reflected in mesoscale activity throughout the recorded channels and that it may have become more reliable across sessions or, in nonimprovers, more noisy in a subset of brain regions.

To assess which electrophysiological signal properties were associated with sequence-specific activity, we performed feature analysis of the spectral features. As γ activity is currently considered a correlate of population spiking activity in mesoscale electrophysiology recordings[8,18], we predicted that γ activity would drive classification performance in all models. We first performed a broad preliminary visual assessment of the importance of all canonical frequency bands and signal property types (amplitude and phase). After verifying the majority of features from different groups were not highly correlated ($\rho > 0.5$), we performed preliminary grouped feature permutation testing (Figure 5D, Figure 5—figure supplements 3 and 4). Collectively, low γ (30–50 Hz), mid γ (50–70 Hz) and high γ (70–250 Hz) appeared to be the most important frequency bands for all models, though the importance of γ phase relative to γ amplitude was inconsistent. Thus, for subsequent formal statistical analysis, we repeated grouped feature permutation testing, except with features grouped into only two groups: 1) δ through β and 2) low γ through high γ (Figure 5E, Figure 5—figure supplement 5). As expected, grouped γ features were the most important to all models. In most brain regions, the direction of across-day change in model performance (Figure 5C) matched the direction of corresponding across-day

change in accuracy drop associated with grouped γ features. Across-day changes in accuracy drop associated with δ through β features were often insignificant, and their direction did not consistently match that of changes in model performance. These findings indicate that sequence-specific activity may have been reflected in distributed γ activity, with γ as the primary driver of across-day changes in classification accuracy for most models.

Improvement is associated with cortically-led δ phase synchrony in response to cue, while possibly pathologically synchronous basal ganglia δ predicts lack of improvement

To understand how oscillatory network dynamics may have contributed to learning-related sequence-specific γ activity, we next characterized δ activity. While there may be sequence specificity in spatiotemporal patterns of neural activity, the overall architecture of functional connectivity is likely sequence-general and learning stage-dependent. We therefore calculated functional connectivity for each sequence and averaged the result across sequences per day before statistical testing, reducing the confounding influence of performance differences between learning stage-matched sequences on a given day. Thus, for functional connectivity, between-day comparisons of neural activity fully mirrored the stratification employed for behavioral analysis. Sequence practice-related effects were those that occurred in overlapping time regions between *both* Days 1 and 3 and Days 3 and 4; though we did not behaviorally stratify task learning, we did examine neural correlates of task exposure by comparing activity between Days 1 and 4.

The excitable phase of δ might reflect a process that facilitates the learning-dependent recruitment of neural ensembles in sequence initiation. If so, we may expect the consistency of event-related δ phase to vary with learning. However, while cortical δ phase has been shown to phase lock to movement-related visual cues[44] and to correlate with reaction time[30,45] in humans, it is unknown whether cue-related δ phase alignment is learning stage-dependent or found outside of cortex. We computed δ phase locking value (PLV)[46] to cue, as all subjects showed δ amplitude sufficient for phase estimation (Figure 6A, Figure 6—figure supplements 1 and 2). In GP subjects, while both GP1 and GP2 demonstrated significant PLV on all days throughout motor cortex and task exposure-related increase in M1 (or M1/S1), only GP1 demonstrated task exposure-related increase in PM. Furthermore, in GP1 but not GP2, PLV was significant on all days in GP and Put, with task exposure-related increase in GP. In STN subjects, PLV was also significant on all days in M1. In other channels (brain regions not surgically targeted in GP subjects), PLV developed differently for STN1 than STN2. In STN1, PLV increased with task exposure in vSTN and Par and with both sequence practice and task exposure in dSTN. In STN2, phase alignment to cue was mostly absent in STN and diminished with task exposure in Par. These results suggest that sequence learning in improvers might have been related to the presence of cue-related δ phase alignment in motor cortex and striatum across days and the development of cue-related δ phase alignment in dSTN with practice; a task exposure-driven enhancement of motor network-wide δ phase alignment to cue occurred in improvers only.

Such anatomically widespread δ phase alignment to cue in improvers suggests cross-area coordinated δ activity, like that proposed to facilitate coordinated recruitment of motor cortical and striatal ensembles with learning in animal models[8]. To assess this, we analyzed interregional δ phase coupling. Using pairwise phase consistency (PPC)[47], we tested for an *increase*, relative to session-wide baseline, in undirected phase coherence aligned to cue and compared PPC between days. When undirected coherence was significant, we compared the phase slope index[48] (PSI; directed coherence) to chance (no channel leads). Two brain regions with a common input could show significant and stable undirected coherence even if a phase lead developed with learning. As undirected coherence exceeded baseline too infrequently to justify systematic between-day PSI testing, we also noted as possibly sequence practice- or task exposure-related any directed coherence that occurred only on specific days (Day 3 for sequence practice; Days 3 and 4 or Day 4 for task exposure).

Only improvers demonstrated cortically-led network δ synchrony, accompanied by M1 lead of dSTN with sequence learning and, with task exposure, possible GP→PM feedback and Par lead of dSTN and M1 (Figure 6B, Figure 6D–E). In GP subjects, only the improver showed widespread cue-related increase in δ coherence above session-wide baseline. On all three days in GP1, PM led M1/S1 and Put, and Put led GP. M1/S1-striatal coherence was relatively low but significant, with phase leads observed for M1/S1→GP and Put→M1/S1. With

task exposure, GP led PM. In GP2, none of these effects occurred. Instead, M1 led PM for familiar sequences. In STN subjects, again only the improver showed cue-related cortically-led δ coherence. In STN1, M1 led dSTN for familiar sequences, and Par led dSTN and M1 with task exposure. Significant cue-related vSTN-dSTN PPC for familiar sequences indicates STN was recruited to network δ synchrony, partly by M1 and perhaps by an unrecorded region. In STN2, no directed phase leads occurred. While vSTN-dSTN PPC was significant for novel sequences, the lack of consistent local δ phase (Figure 6A) indicates that inter-STN coherence was suboptimal for coordinated phase coding. Notably, in both nonimprovers, inter-BG δ synchrony was initially high and decreased with task exposure—an effect mirrored in session-wide inter-BG δ coherence, opposite that observed in improvers (Figure 6C). High inter-basal ganglia δ synchrony in nonimprovers was linked to limited cue-related BG δ activity, an absence of cortico-basal ganglia δ synchrony and reversal of motor corticocortical δ information flow.

Sequence learning is associated with δ-γ coupling within and between cortex and basal ganglia

Having found evidence for cue-related coordinated δ activity to support the learning-dependent sequence-specific γ activity detected with single-trial classification, we next tested the δ→γ component of the β→δ→γ framework. Work in animal models suggests that δ coupling with motor ensemble spiking may occur locally within basal ganglia and motor cortex and between these regions[13,34,49], so we tested both intraregional and interregional δ phase-high γ coupling (Figure 7). Using pairwise phase consistency and phase slope index, we calculated undirected and directed coherence between δ phase and the δ phase of the γ amplitude envelope (γ_h^δ). For interregional CFC, we report all results for which at least one subject demonstrates an effect of either sequence practice or task exposure.

In these subjects, local δ→γ_h^δ coupling did not appear to be a necessary step in general motor initiation. In no channels did any δ-γ_h^δ directed coupling occur across all days (Figure 7—figure supplement 1). Nonetheless, M1 high γ amplitude still significantly increased in the RT period on all days in all subjects (Figure 7—figure supplement 2), as expected for successful movement[19,20]. While δ locally led γ_h^δ in two brain regions on Day 1 (GP2's GP and STN1's Par), implying possible involvement of δ in facilitating their sequence-specific γ activity on Day 1 (Figure 5), this effect was inconsistent across days. Instead, in a practice-dependent manner, local γ activity may have helped coordinate δ in some cortical areas for some individuals. These results suggest that local δ→γ_h^δ coupling was unlikely to have directly facilitated much of the observed sequence-specific γ activity in classification analysis.

While interregional δ→γ_h^δ coupling also did not appear to be a necessary step in general motor initiation, sequence practice-related δ-γ_h^δ coupling patterns differed between the improver and nonimprover within both GP and STN subject groups (Figure 7A–B). In GP1 but not GP2, sequence practice was associated with premotor lead of M1/S1, as well as M1/S1 and PM lead of putamen. In STN1 but not STN2, sequence practice was associated with dSTN lead of M1 and vSTN, as well as M1 lead of Par. In STN2, Par instead led M1 on Days 1 and 3, but this effect was gradually lost with task exposure. Otherwise, there were no task exposure-related effects in any subjects. Notably, δ led γ_h^δ only for M1 γ_h^δ with sequence learning in improvers, potentially contributing to the improvement-related increase in discriminability of M1 sequence-specific γ activity (Figure 5). Together, these results associate sequence learning with a range of interregional δ-γ_h^δ effects that differ depending on the involved brain regions.

With sequence practice and task exposure emerge unique patterns of δ-β coupling

Using the same approach, we finally tested the β→δ component of the framework and its learning stage dependence by assessing coupling between δ phase and the δ phase of the β amplitude envelope (β^δ). The release of cortical δ could be led by cortical β, subcortical β or a combination of both. Thus, we assessed both intraregional and interregional δ-β^δ coupling (Figure 8).

Though there was substantial overlap of regions with consistent movement-related β desynchronization and regions with cue-related δ phase alignment (all motor regions in improvers; motor cortex and putamen in nonimprovers) (Figure 6A, Figure 8—figure supplement 1), this overlap was infrequently associated with local δ-β^{δ} directed coupling (Figure 8—figure supplement 2). While there were some possibly practice- or task exposure-related effects, in no channels did any δ-β^{δ} directed coupling occur across all days. Furthermore, in motor cortex, the presence and direction of coupling were inconsistent across subjects, suggesting that local cortical δ-β^{δ} coupling might not have been a consistent gating mechanism in these subjects.

Our evaluation of interregional δ-β^{δ} coupling suggests that interregional β→cortical δ coupling was also not a consistent general initiation mechanism in these subjects and, instead, that interregional δ-β^{δ} coupling developed uniquely with sequence practice and task exposure (Figure 8A–D). While some corticocortical β^{δ} lead of δ developed with task exposure in most subjects, it was never present across all days. In GP subjects, sequence practice was associated with striatocortical δ-β^{δ} coupling in GP1, as opposed to corticostriatal δ-β^{δ} coupling in GP2 (Figure 8A–B). With task exposure, primary motor cortex led PM in both GP subjects, but only in GP1 was GP led by all recorded brain regions (Put, M1/S1, PM) (Figure 8C–D). In STN subjects, no sequence practice-related effects were observed. However, with task exposure in STN1, Par led M1 and dSTN, while no effects were observed in STN2. These results associate sequence learning with striatocortical δ-β^{δ} coupling and link task exposure to a range of anatomically-specific δ-β^{δ} couplings within and between cortex and basal ganglia—almost all effects of which were absent in nonimprovers.

DISCUSSION

This study investigated learning-dependent neural dynamics of motor sequence initiation in PD. Though all subjects demonstrated M1 β desynchronization, δ phase response and γ synchronization, in no subjects was a cascade of β→δ→γ consistently present—possibly reflecting PD-related neuropathophysiology. However, consistent with the prediction that γ activity can reflect learning-related changes in ensemble activity, we detected learning-dependent sequence-specific γ activity. Sequence-specific γ activity was discriminable in all brain regions and, with practice, predictive value increased in improvers but decreased in nonimprovers. Consistent with the idea that coordinated δ may facilitate enhanced neural ensemble recruitment, in improvers, increasing predictive value of M1 γ was accompanied by δ→M1 γ coupling, led by brain regions synchronized with M1 δ. More broadly, unique patterns of functional connectivity emerged with sequence learning and task exposure in improvers, linked by a common framework of cortically-led δ synchrony (Figure 9). In contrast, nonimprovers exhibited highly coherent basal ganglia δ, which showed inconsistent responses to cue and coincided with minimal functional connectivity—suggesting that pathologically synchronized BG δ could interfere with motor learning in part due to its reduced sensitivity to cortical input. These findings support a model for sequence initiation in PD wherein cortically-led network δ reflects an organizing network process common to sequence and task learning, with the two learning types distinguished by a unique interplay of δ synchrony and CFC.

Central limitations

While our study demonstrates meaningful advances, it is limited by a small sample size. Recordings in GP and STN subjects were largely anatomically nonoverlapping, enabling observation of the unique roles of various brain regions but leaving unverifiable the consistency of effects across improvers or across nonimprovers. That half of subjects did not improve enabled stratification of subjects by improvement status, but the resulting $n = 1$ per learner type per brain region necessitated reliance on within-subjects comparisons. Consequently, conclusions based on comparison of improvers and nonimprovers are inherently weak and may not generalize, as is often the nature of work in invasive human electrophysiology.

One surprising behavioral observation was that, from the start, nonimprovers moved at least as quickly as improvers, indicating that lack of improvement in nonimprovers was not likely due to greater difficulty in manipulating the keyboard. Nonimprovers may have found the task too easy at baseline to show measurable

speed increases across days, despite actually learning the sequences. However, while improvers' single-trial trial durations frequently demonstrated performance decrement when switching between sequences within day, suggesting a sequence switching effect indicative of sequence learning, this effect was less apparent in nonimprovers. Alternative explanations are that improvers had more bradykinesia; that improvers more effectively learned sequences during task familiarization prior to the experiment, resulting in greater impact of interference from familiarization sequences on Day 1 movement speed; or simply that the speed differences reflect typical inter-individual variability prior to learning.

Finally, the complex nature of the system and the form of recording and analyses employed introduce considerable room for bias, particularly in interpreting data from bipolar montages spanning multiple brain regions and in interpreting cross-frequency and directed coherence. Large task exposure-related effects may have obscured smaller overlapping effects of sequence practice, and learning-related functional connectivity likely also occurs in frequency bands beyond those addressed herein.

Future studies should aim to replicate these findings in a larger cohort and to explore the impact of Parkinson's Disease stage and treatment modalities.

The β→δ→γ framework for motor initiation: an assessment in Parkinson's Disease

Previous work suggests that pathologically high levels of network β synchronization seen in PD may interfere with movement initiation[19,50–52] by delaying release of cortical excitability[21,53] and thereby delaying the facilitation of high-frequency cortical activity associated with movement production[8,19,20,32,33,54–56]. This suggests that general motor initiation involves a basal ganglia or cortical β→cortical δ→cortical γ cascade, which was absent in our subjects, perhaps as a result of PD. While some cortical β→δ and δ→γ coupling developed across days in some individuals, only once was the specific pattern of couplings consistent with a cascade: in STN1 on Day 4, as M1 β and Par β led M1 δ, which, in turn, led M1 γ. One of the most noteworthy findings was the prevalence of γ→δ coupling in cortex, both locally and interregionally. This direction is opposite of that which we predicted, but most studies assessing δ coupling with γ or with spiking activity have assessed only undirected coupling[49,57–59]. The local motor cortical δ-γ coupling we observed could have been compensatory or pathological, related to a rise in cortical δ sometimes seen with PD progression[60–62]—analogous to the coincidence of elevated cortical δ and disrupted δ-spike coupling after stroke, which recovers alongside motor improvements[8]. Nevertheless, our subjects still successfully initiated movement, indicating that the gating framework might only describe contributing, rather than prerequisite, factors to motor initiation in some individuals.

Practice-driven pre-movement sequence-specific activity

Though pre-movement sequence-specific activity has been observed in nonhuman primate motor cortex[10,11], there has been limited electrophysiological investigation of pre-movement sequence-specific activity in the human brain. Decoding analysis of pre-movement neural activity revealed sequence specificity throughout the recorded network in all subjects on all days, indicating that all recorded brain regions may have reflected a sequence-specific initiation signal regardless of learning stage. Considering the within time-frequency percentile feature selection and the lasso regularization, that γ activity was found to be the most important frequency band was not likely due simply to the higher number of γ center frequencies than lower frequency bands pre-selection. Thus, given between-contact subtraction in our bipolar recording configuration, γ might have reflected sequence specificity in the relative amplitudes and timings of activity in ensembles most proximal to one or both of the contacts[18,63].

Changes in classification accuracy of sequence-specific activity could likewise indirectly relate to changes in variability of local sequence-specific ensemble activity. If so, we would expect increasing classification accuracy in subjects who show behavioral improvement[14–16] and for increases to be associated with δ synchrony and enhanced δ→γ coupling[8,13]. Consistent with these expectations, we observed across-day

increases in predictive value in almost all brain regions in improvers, for whom motor network-wide δ synchrony also developed. For primary motor cortex, this was associated with enhanced δ→γ coupling (PM→M1/S1 and dSTN→M1). Inconsistent with these expectations, we did not observe learning-related δ→γ coupling for other regions. It is possible that unrecorded regions contributed to the increase in γ's predictive value. Alternatively, δ could have influenced sequence-specific activity indirectly through its lead of β, which has also been proposed to bind together action plan-specific neural ensembles across the motor network[8]. That motor performance did not worsen with decreasing classification accuracy in nonimprovers suggests that any increased variability in ensemble activity may have been sufficient to prevent improvement but insufficient to cause a significant performance decline; alternatively, the impact may have been offset by compensatory mechanisms.

Importantly, these suppositions are ultimately conjecture. Given our small sample size and recordings at the level of populations rather than individual neurons, this predictive analysis may best serve as a recommendation system to inspire future experimental work.

Unique patterns of cortico-basal ganglia coupling in sequence learning and task exposure in improvers

Sequence learning and task exposure were associated with distinct changes in cross-frequency activity in improvers. Most notably, while both sequence learning and task exposure involved a range of corticocortical, cortico-basal ganglia and inter-basal ganglia effects, only sequence learning involved basal ganglia→cortex CFC. In fact, basal ganglia→cortex CFC occurred only in improvers, only with sequence learning and only involving dSTN and putamen δ. This is broadly consistent with models of the cortico-basal ganglia system implicating these regions in motor learning and action selection[2,64–70], is consistent with the possibility that pre-movement δ→β and δ→γ are associated with enhanced neural pattern organization, and centers basal ganglia feedback during motor initiation as a possible factor in motor improvement[33].

Changes in δ synchrony also differed for sequence learning and task exposure. Enhanced network synchrony with motor learning aligns with human neuroimaging studies showing learning-related corticostriatal connectivity[71–73] and with animal model studies suggesting corticostriatal tutoring[74–76]. We established a cortex→striatum direction of lead, which was present consistently throughout the experiment, and found sequence learning-related M1→dSTN connectivity. In contrast, task exposure involved the development of parietal lead of M1, which aligns with S1→M1 activation previously detected in a human ECoG study of finger movements, suggestive of a predictive efference copy[77]. Another notable effect of task exposure was the development of GP→PM δ synchrony, which developed concurrently with motor cortical β lead of GP δ and of PM δ. As δ phase coordination then occurred for PM→putamen, putamen→GP and GP→PM, this suggests that a cortico-basal ganglia loop of δ phase coordination, in part facilitated by cross-frequency input from cortical β, could reflect an electrophysiological substrate for the manifestation of general motor familiarization or task learning-related attentional processes[57,78–80], which could facilitate greater ease of future sequence learning.

Perhaps the most apparent inconsistencies between ours and previous work relate to a rodent study of the reach-to-grasp (RTG) task[34]. Lemke et al. found that low-frequency (3–6 Hz) corticostriatal LFP activity was essential to motor learning—along with concurrent development of low-high frequency interregional coupling—but not present during skill acquisition and not important to the dexterous component of movement. These discrepancies could result from differences in learning stage or type. The rodents learned a novel grasping task without extensive prior motor familiarization, whereas our subjects had typing experience and a full task run-through before the experiment. Our task also required learning the serial order of individuated digit movements, which is thought to rely on striatum in primates[81]—a key component absent in rodent RTG. Taken together, our studies suggest that corticostriatal low-frequency synchrony may be related to both the initiation of externally cued dexterous movements and the execution of coarse movements.

Few effects of sequence practice and task exposure in nonimprovers: a possible role for pathologically synchronized basal ganglia δ

In nonimprovers, all effects of sequence practice seen in improvers were absent, and there were strikingly few neural correlates of task exposure. All observed sequence practice- or task exposure-related effects occurred in GP2 and involved M1 leading PM and GP. This is consistent with the fact that GP2 exhibited trending performance improvement and suggests that some sequence learning occurred through M1 compensatory processes[82,83], insufficient to drive detectable changes in behavior, or that some observed M1 activity was maladaptive[84]—possibly both. In STN2, while the lack of any gained across-day effects could have been due to quantitative limitations related to STN2's relatively short reaction time window, we still detected the loss of various effects across days, indicating that the length of STN2's RT window did not prevent detection of functional connectivity. That both sequence practice- and task exposure-related effects involving subcortical δ in improvers were absent in nonimprovers highlights a possible role of cortico-basal ganglia δ communication in both processes and, likewise, suggests possible interdependence of these processes that warrants future study.

The shared absence of sequence practice- and task exposure-related effects involving BG δ may have been related to high session-wide inter-basal ganglia δ synchrony. Human and animal studies have detected δ-range spiking activity in GP and STN in low dopamine states, which could represent either a low tremor frequency[85,86] or a unique biomarker of motor symptoms[87]. Either case proposes that ineffective therapeutic recovery of BG dopaminergic transmission permits pathological δ activity. However, although subjects exhibiting elevated BG δ synchrony were those with higher pre-experiment total MDS-UPDRS scores on medication (Table 1), their daily post-task UPDRS upper limb scores were comparable to those of other subjects and demonstrated no apparent across-day drop alongside the across-day decrease in BG δ synchrony (Table 3). It is possible that task exposure drove the across-day BG δ synchrony decrease to promote the possibility of future learning and that the MDS-UPDRS upper limb component was too insensitive[88] to detect associated changes in hallmark upper limb motor symptoms. Alternatively, temporary functional lesion from subcortical lead insertion may have temporarily increased δ, similar to the effect of cortical stroke[8]. Given the small sample size and inherent inter-individual variability, it is possible that, by chance, BG δ had recovered in improvers before the start of the experiment, while nonimprovers had longer BG δ recovery timelines, in part leading to the learning differences between these groups. In any case, the concurrent lack of improvement and lack of sequence practice- or task exposure-related effects involving BG δ suggests that event-related coordination of basal ganglia δ may have been crucial to motor learning in these subjects.

Coordinated network δ as a possibly facilitatory network state for learning-dependent cross-frequency coupling during sequence initiation

From the theoretical standpoint, δ is an ideal substrate for information multiplexing, local gain modulation and information transfer between distant phase-aligned brain regions[27,29,78–80]. Experimental evidence supports this, showing a role for δ in information sequencing through phase-specific ensemble patterning[13,34]; sensory integration and attentional control through gain modulation achieved by changes in neural excitability[29,30,89,90]; and functional network organization, information transfer and distributed representation through cross-area coordinated activity that coactivates distributed ensembles[13,27,34,59,91].

Consistent with these roles, in our study, cross-area coordination of δ phase may have formed the infrastructure for a cue-responsive network state, within which learning-related δ-β and δ-γ coupling developed. While δ synchrony and phase alignment to cue occurred on Day 1 and increased across days, directed δ-β and δ-γ couplings were initially mostly absent. Only brain regions that demonstrated δ phase alignment to cue contributed δ to interregional δ→β or δ→γ coupling, and β and γ lead of δ was often associated with the recipient δ demonstrating enhanced cue alignment or enhanced lead of other brain regions (e.g., task exposure-related effects in GP1's GP), suggesting a possible learning-dependent role for β and γ in the organization of network δ.

This link between motor performance-related δ activity and CFC is consistent with lesion experiments in animal models[13,34] and observational studies of the human cortical grasp network[59]. Other work has found reaction time-correlated cue-responsive δ phase reset in human hippocampus[92], reaction time-correlated δ phase in rat motor thalamus coupled to local spiking[93], motor learning-related M1-cerebellar δ synchrony in rats with enhanced cross-area spiking activity[94] and even evidence for prefrontal guidance of motor plans via δ-β coupling in humans[95]. Coordinated δ may ultimately reflect a motor system-wide neural process facilitating local and distributed activity patterns over the course of learning.

An important question is what neurophysiological activity is actually reflected in spectral estimates of δ recorded with mesoscale electrophysiology, and the answer may be a combination of multiple possibilities. While δ has been associated with excitability and with single-unit spiking at δ frequency, it has also been linked to the dynamics of population spiking activity[49,96], similar to γ, and it could reflect synaptic input[97–100]. It is thus important to clarify that δ activity may not directly drive other neural activity, per sé, but rather reflect the dynamics of some component of the underlying process that is directly responsible for driving the observed network effects.

Clinical implications

To the best of our knowledge, this study is the first invasive electrophysiological investigation of human cortico-basal ganglia dynamics in motor sequence learning and possibly the first formal evaluation of isolated fine motor sequence learning in PD across multiple days of practice. Our findings help clarify the intricate and dynamic functional architecture of the human motor control network in the initiation of fine motor sequences in Parkinson's Disease and posit neurostimulation directed at coordinating cortico-basal ganglia δ synchrony as a therapeutic neuromodulatory strategy targeting the initiation of fine motor skills.

Conclusion

In individuals experiencing Parkinson's Disease, we outline a hierarchical, learning-dependent functional architecture of oscillatory cortico-basal ganglia activity for the initiation of fine motor sequences. The findings illuminate how disparities in information content and flow may relate to disparities in motor learning outcomes. Extending this work in larger cohorts of individuals with PD could help elucidate the relationship between clinical characteristics and practice-related neural dynamics and further clarify the potential for phase-specific basal ganglia stimulation to modulate pathological neural dynamics in the production of fine motor skills.

MATERIALS AND METHODS

Study Criteria

Four individuals enrolled in parent clinical trials (NCT03582891 and NCT04675398) for adaptive deep brain stimulation (DBS) for Parkinson's Disease (PD) participated in this study. For overarching clinical trial inclusion and exclusion criteria, see NCT03582891 and NCT04675398. Additional prescreening was performed for the typing task. Inclusion criterion: enthusiastic desire to participate in the task. Exclusion criteria: hand or wrist pain when typing, dyslexia, uncorrected visual impairment, sleep apnea, travel to the eastern hemisphere in the past three months. Subjects were also instructed not to consume nicotine or alcohol for the duration of the experiment. Subjects gave informed consent, and the University of California San Francisco Institutional Review Board pre-approved experimental design.

Task Design

On each day of a multi-day explicit motor learning experiment, subjects practiced typing two 5-element sequences in interleaved blocks using their dominant (right) hand while neural activity was recorded from the contralateral hemisphere (Figure 3A). The task design within each day was a variation of the common discrete sequence production task[101]. In the Verification Period, subjects were briefly shown one sequence to memorize before typing it from memory repeatedly until three consecutive fully correct repetitions were achieved. This was repeated with the second sequence. After completing the initial Verification Period, subjects were instructed to, in the subsequent practice blocks, react as quickly as possible to each go cue and to type as quickly and accurately as possible. Each subsequent practice block started with its own Verification Period for the sequence for that block. Then, subjects typed the sequence from memory once in response to each exponentially jittered occurrence of the green go cue (range: 0.85s–3.75s, $\mu = 1.75$, $p = 0.4$ for Lilliefors test for $h0$ = exponential). A 10-second break occurred after each block. Subjects' hands and the keypad were completely visually occluded, and the sequences were never displayed during typing. No sequences contained repeated adjacent elements, rising or falling triplets, or the thumb. All sequences paired for comparison within and between days started with the same first and last elements.

Data Collection

In each brain hemisphere, a four-contact DBS lead spans basal ganglia (BG) nuclei, and a four-contact electrocorticography (ECoG) paddle overlays sensorimotor cortex (Figure 2). Leads from each brain hemisphere (Medtronic 3387 for globus pallidus, 3389 for subthalamic nucleus and 0913025 for cortex) were connected to a bidirectional neural interface in the ipsilateral chest (Medtronic Summit RC+S B35300R). LFP and ECoG signals from the left (contralateral) brain hemisphere were recorded throughout the task at 500 Hz from four bipolar contact pairs per brain hemisphere: two channels in basal ganglia and two in sensorimotor cortex. Channels were referenced to the metal casing of the implanted pulse generator. On-device hardware low and high pass filtered the data at 450 Hz and 0.85 Hz, amplified it, then performed another low pass filter at 1700 Hz.

Task events and keystroke data were captured in 4-kHz sweeps using a portable custom-made device run by a Teensy 4.1 microcontroller (Figure 3C), which acted as the master clock and motherboard for a custom keypad, visual stimulus detector and electrical impulse detector. To ensure accurate detection of finger movement onset/offset, even when finger position started above but not touching the key, a combination of custom capacitive proximity sensors (carved from copper sheet metal, 3DDeluxe), force-sensitive resistors (FSRs, Alpha MF01A-N-221-A04) and linear mechanical key switches (CHERRY MX1A-LxxA/B) were used for each digit. An FSR was fixed atop each custom keycap (3DDeluxe).

A small resin disk with a bulge less than a millimeter tall in the center was fixed atop each FSR; this helped to ensure that off-center finger contact with the key face would still produce FSR activation by redistributing some

of the applied force to the FSR's center active zone. The resin disks also insulated the FSRs from the proximity sensors, which were cut from copper sheet metal and fixed atop each resin disk. To maximize proximity sensor read rate, each proximity sensor was sampled by its own Teensy 3.2 microcontroller, each of which transmitted readings to the Teensy 4.1. Proximity sensors were covered with insulating tape and calibrated to detect proximity changes of fingers hovering up to ~2 cm above the keys. The capacitance sensors could also detect changes in surface area of finger contact with the key, even for changes slight enough that the associated change in force was subthreshold for the force sensors. A photodiode (Everlight Electronics Co Ltd, PD333-3C/H0/L2) fixed to the task computer screen captured the timing of visual stimuli and progression of experimental epochs. A unique temporal pattern of fifteen single DBS pulses was delivered at the start and end of each experimental session and detected along the metal casing of the pulse generator by an electrical signal detector (MikroElectronika EEG Click MIKROE-3359) for neural-behavioral data stream alignment. All sensors were calibrated and checked for electrical interference and cross-talk at the start of each experimental session.

Behavioral Analysis

To eliminate outlier trials, we excluded incorrect trials and any trials with a reaction time (RT, cue onset to movement onset) or trial duration (movement onset to offset) exceeding three standard deviations of the block average for correct trials.

A performance index was calculated per block to compare the overall performance levels of sequences within and across days for a given subject. All block average error rates (1 – accuracy) for Days 1–4 were compiled and min-max scaled to [0, 1] per subject. This was repeated for block average reaction times and block average trial durations. For each block, the resulting scaled average error rate, reaction time and trial duration were summed. Therefore, the performance index range is [0, 3], where lower value indicates better relative performance.

Neural Analysis

All significance testing for neural analysis utilized permutation testing that simulates error within the null distribution, and secondary tests were performed only to assess the direction of primary detected effects. Multiple comparison correction was therefore not performed.

Trial Selection

In addition to the behavioral cutoffs applied for behavioral analysis, the following trial exclusion criteria and trial subsampling methods were performed for neural analysis. Trials with less than 25 ms between final/first movements associated with adjacent trials were excluded. Subsequently, subsampling was performed within a given day to match trial counts between sequences within each group of four blocks to avoid a possible imbalance over time, e.g., 75% of remaining Sequence 1 (S1) trials coming from the first half of the session and 75% of remaining Sequence 2 (S2) trials coming from the second half of the session. Within each group of four blocks, sequence subsampling followed epoch-specific selection rules. Only trials with RT ≥ 100 ms were considered. Trials from the higher count sequence were subsampled to match trials from the lower count sequence based on RT durations. Finally, random subsampling matched trial counts across days within each subject for each epoch type.

Signal Preprocessing

Neural signal preprocessing used the following pipeline. Data from each channel was linearly detrended, demeaned and high-pass filtered at 0.25 Hz using a two-pass FIR filter. Electrical noise was excluded in the frequency domain. Two-pass Kaiser FIR filters with normalized transition widths of ≤ 0.1 were used for all subsequent bandpass filtering.

Data intended for single-trial classification, amplitude analysis and undirected phase analysis was filtered with the following passbands: δ (0.5–4 Hz), theta (4–8 Hz), alpha (8–12 Hz) and β (12–30 Hz for amplitude analysis and cross-frequency coupling, 12–20 Hz and 20–30 Hz for single trial classification). For γ, filters were logarithmically spaced from 30 to 250 Hz. High γ (70–250 Hz) center frequencies were used for all analyses involving γ, while slow (30–50 Hz) and mid (50–70 Hz) γ center frequencies were used only for single-trial classification. These filters were all non-overlapping in the frequency domain to reduce collinearity between adjacent frequency bands when performing single-trial classification. The Hilbert transform was performed for instantaneous frequency estimation. For undirected cross-frequency coupling (CFC) analysis using pairwise phase consistency (PPC), the resulting amplitude envelope of each β and γ center frequency was filtered with the same bandpass filter previously used to extract δ, followed by a second application of the Hilbert transform.

For analysis of directed phase coherence (including directed CFC) using phase slope index (PSI), δ was instead extracted using linearly spaced passbands (0.5, 3.25; 0.75, 3.5; 1, 3.75; 1.25, 4). For directed δ-β and δ-γ coupling analysis, these linearly spaced δ passbands were applied to the β amplitude envelope and to the amplitude envelope of each center frequency of high γ (70–250 Hz), followed by a second application of the hilbert transform.

For artifact screening, filter-Hilbert was used to estimate 70–250 Hz broadband amplitude, which was then *z*-scored over the entire session. Any trial in which *z* ever surpassed 8 standard deviations was omitted from neural analysis.

Single-Trial Classification

A different classifier was trained on data from each recording channel on each day, and mean decoding accuracy was used to estimate the discriminability of sequence-specific neural activity. To test for sequence-specific activity immediately prior to sequence initiation, S1- or S2-labeled trial data was extracted from the RT period in the t_n ms immediately prior to sequential movement onset, where t_n was the average RT on Day 3 for Subject *n*. Data then underwent feature selection and logistic classification with L_1 regularization. For each subject, trials per sequence were balanced across classes, channels and days.

Time-frequency regions with maximal differences between sequences were selected as features (Figure 5A-B). To assess, e.g., differences in narrowband amplitude dynamics in PM for S1 vs. S2 on Day 3 for GP1, we calculated the two-sided *t*-statistic for amplitude at each time-frequency point. For each of 10,000 permutations, trial labels were shuffled, and the *t*-statistic was recalculated. Thus, each time-frequency point had an associated null distribution of 10,000 *t*-statistic values. Time-frequency points at which the test value fell below the 80th percentile compared to its respective null distribution were masked. In each of the remaining islands of features for each center frequency, the time point with the highest percentile score relative to its null was selected as a feature to use in the model. For all resulting features, corresponding amplitude values were taken from S1 and S2 trial data. For phase data, the same process was implemented, save for two differences. Phase opposition sum[43] was used instead of the *t*-statistic, and since phase is a circular process, each selected phase value was converted into two features: sin(phase) and cos(phase). Each amplitude and phase feature was median-centered and scaled according to its interquartile range to have unit variance.

Hyperparameter optimization, model training and model testing were performed with nested cross validation. The inverse L_1 regularization constant (λ^{-1}) was optimized per classifier in 10-fold, 10-repeat stratified cross validation performed on a stratified 90% subset of the data. The following λ^{-1} values were tested: 5E-2, 1E-1, 5E-1, 1, 5, 1E1, 5E1, 1E2, 5E2, 1E3, 5E3, 1E4, 5E4, 1E5, 5E5. Greater shrinkage produced performance at or

below chance level. The selected value for λ^{-1} was then used for final model training and testing on the full dataset with 10-fold, 100-repeat stratified cross validation.

Right-sided permutation testing assessed significance of model mean decoding accuracy relative to chance. The outer 10-fold, 100-repeat stratified cross validation was repeated 1,000 times with permuted trial labels, and the resulting 1,000 null values were compared to test sample mean decoding accuracy.

Two-sided permutation testing assessed the change in mean decoding accuracy across days for a given channel. Mean decoding accuracies for each of the 100 repeats per day were permuted across days, and the between-day difference in overall mean decoding accuracy was recalculated for each permutation as the null value.

Feature Importance Testing

For Figure 5D and Figure 5—figure supplement 4, the absolute importance of various frequency bands and signal properties to the performance of trained models was evaluated. We permuted, in the test set, the trial labels for all phase *or* amplitude features associated with a given canonical frequency band, as the majority of across-frequency or across-phase/amplitude feature correlations were not high ($\rho < 0.5$) (Figure 5—figure supplement 3). For each fold in each repeat of the 10-fold 100-repeat outer cross-validation used for prior model training and testing, the test data trial labels for the respective trained model were permuted once for a given feature group, and the resulting change in test accuracy from test performance was computed. Change in decoding accuracy was then averaged across all 10 folds in each of the 100 repeats. Feature groups that showed negligible negative accuracy decreases were set to zero in the plots for Figure 5D and Figure 5—figure supplement 4 for the purpose of clarity in data visualization. No groups showed a negative accuracy decrease greater than 1% in any model.

For Figure 5E, we repeated group permutation testing, except with all phase and amplitude features for δ through β grouped together and likewise for low γ through high γ. Change in decoding accuracy was averaged across folds per repeat before between-day permutation testing.

Coherence Analysis

Single-trial plots indicated that δ phase aligned to cue in various regions (Figure 6—figure supplement 2), so data was aligned to cue and evaluated in a window length of the mean RT of Day 3 per subject. Nonparametric cluster-based permutation across time, with a cluster size correction, was used for all phase analyses.

For all phase analyses, we first computed each metric within sequence before averaging the resulting time series across sequences prior to statistical testing. This was intended to address two main issues. First, we expected possible sequence-specificity in spatiotemporal patterns of neural activity that could be reflected in mesoscale spectral activity—an idea for which both single-trial classification and single-trial δ phase plots then provided confirmatory evidence (see sequence specificity in absolute phase of δ for GP1 M1/S1, Figure 6—figure supplement 2). This implies that different sequences could be associated with different characteristic γ amplitude envelope morphologies, which may display different phase-specific coupling patterns with δ. Second, in cases for which two sequences were not performance-matched on a given day (e.g., Sequences 3 and 4), one may observe differences in activity between sequences due to performance level (rather than learning stage). In either case, a reasonable approach would be to respect the sequence-specific relationships, so we first computed metrics within each sequence. However, we also expected the general oscillatory network dynamics associated with learning to be the same regardless of sequence, so we then averaged the resulting metric time series across sequences before statistical testing.

Inter-trial δ phase locking value (PLV)[46] assessed cue-aligned consistency of local δ phase. For a given recording channel, the resulting time series (one for each sequence) were smoothed with a 150 ms-long

Gaussian window and averaged across sequences. To test for significant PLV on a given day, we randomly sampled phase data from the duration of the session for each permutation. PLV was computed for each sequence null group using the appropriate number of trials for each sequence. The magnitudes of the resulting two null PLV time series were then smoothed and averaged across trial groups to attain a single null time series for that permutation. This was repeated for each permutation. To test for a significant difference in PLV time series between days, we calculated the test time series by subtracting the PLV time series from one day from that of the other day. For each permutation, trials were shuffled across days but within sequence.

Inter-trial δ pairwise phase consistency[47] assessed cue-aligned interregional δ phase coherence. For each channel pair, the resulting time series (one for each sequence) were smoothed with a 150 ms-long Gaussian window and averaged across sequences. For baseline PPC testing, methods were identical to those used in baseline PLV testing, except the null was constructed by sampling channel data as pairs, i.e., the baseline distribution corresponded to an actual estimate of baseline session-wide coherence for that channel pair, not to the level of coherence that would be expected if the two channels were coupled only randomly. For between-day PPC permutation testing, test time series were calculated by subtracting the PPC time series between days, and for each permutation, phase data for both channels in a given channel pair were shuffled together across days but within sequence.

To assess the direction of pairwise δ phase relationships observed with PPC, phase slope index[48] between two channels was computed per time point for each sequence. PSI values were not smoothed before being averaged across sequences. To assess whether significant δ phase lead/lag occurred with respect to chance, i.e., neither channel led the other, rather than with respect to session baseline, data for each permutation was randomly sampled from the session duration separately for each channel in the pair, for each sequence.

Pairwise phase consistency and phase slope index were also used to estimate undirected and directed coherence, respectively, for cross-frequency couplings. δ phase was paired with the δ phase of the β or γ amplitude envelope. Computations analogous to those used for δ synchrony analysis were performed, except for two modifications. For δ-high γ coupling, PPC or PSI was calculated separately for each narrowband within 70–250 Hz for each sequence. The result was averaged across γ center frequencies before averaging across sequences. Second, for baseline permutation testing, the phase data was held constant while the amplitude data was sampled from the session. Shuffling amplitude while holding phase constant was intended to test for significant coherence *given* a specific phase distribution.

Use of artificial intelligence tools

DALL-E was used to generate the first draft of the hand in Figure 3A. After initial drafting of the manuscript, ChatGPT and Gemini were used to help improve the concision of the text during editing.

AUTHOR CONTRIBUTIONS

K.N.P. developed the experimental setup, including designing and fabricating custom behavioral hardware, programming firmware and developing protocols for neural-behavioral recording and alignment. K.N.P. performed the experiment. K.N.P. collected sleep journals and administered daily upper limb component of the MDS-UPDRS. K.N.P. performed all data curation, processing and analyses. K.N.P. and D.D.W. designed the experiment. K.N.P., R.A. and T.A.W. developed quantitative methodology. K.N.P. and K.H.L. set visual stimulus presentation. S.L. scored the UPDRS videos. D.D.W. and P.A.S. performed the neurosurgeries and funded the parent clinical trials. T.A.W. performed lead reconstruction. K.N.P. wrote the manuscript. All authors reviewed the manuscript.

ACKNOWLEDGEMENTS

We thank the members of the OpenMind Consortium and the D.D.W., R.A., P.A.S. and S.L. laboratories for valuable discussion over the course of the study. We thank Rich Ivry for helpful guidance during experimental design and data interpretation, as well as critique of the manuscript. We thank Karunesh Ganguly for thoughtful advice during data interpretation and critique of the manuscript.

REFERENCES

1. Udupa K, Bhattacharya A, Bhardwaj S, Pal PK, Chen R. Chapter 9 - Parkinson's disease: Alterations of motor plasticity and motor learning. In: Quartarone A, Ghilardi MF, Boller F, eds. *Handbook of Clinical Neurology*. Vol 184. Neuroplasticity. Elsevier; 2022:135-151. doi:10.1016/B978-0-12-819410-2.00007-2
2. Marinelli L, Quartarone A, Hallett M, Frazzitta G, Ghilardi MF. The many facets of motor learning and their relevance for Parkinson's disease. *Clin Neurophysiol*. 2017;128(7):1127-1141. doi:10.1016/j.clinph.2017.03.042
3. Ariani G, Diedrichsen J. Sequence learning is driven by improvements in motor planning. *J Neurophysiol*. 2019;121(6):2088-2100. doi:10.1152/jn.00041.2019
4. Ariani G, Kordjazi N, Pruszynski JA, Diedrichsen J. The Planning Horizon for Movement Sequences. *eneuro*. 2021;8(2):ENEURO.0085-21.2021. doi:10.1523/ENEURO.0085-21.2021
5. Verwey WB, Shea CH, Wright DL. A cognitive framework for explaining serial processing and sequence execution strategies. *Psychon Bull Rev*. 2015;22(1):54-77. doi:10.3758/s13423-014-0773-4
6. Wong AL, Haith AM, Krakauer JW. Motor Planning. *The Neuroscientist*. 2015;21(4):385-398. doi:10.1177/1073858414541484
7. Verwey WB. Evidence for the development of concurrent processing in a sequential keypressing task. *Acta Psychol (Amst)*. 1994;85(3):245-262. doi:10.1016/0001-6918(94)90038-8
8. Ganguly K, Khanna P, Morecraft RJ, Lin DJ. Modulation of neural co-firing to enhance network transmission and improve motor function after stroke. *Neuron*. 2022;110(15):2363-2385. doi:10.1016/j.neuron.2022.06.024
9. Carrillo-Reid L. Neuronal ensembles in memory processes. *Semin Cell Dev Biol*. 2022;125:136-143. doi:10.1016/j.semcdb.2021.04.004
10. Lu X, Ashe J. Anticipatory activity in primary motor cortex codes memorized movement sequences. *Neuron*. 2005;45(6):967-973. doi:10.1016/j.neuron.2005.01.036
11. Hatsopoulos NG, Paninski L, Donoghue JP. Sequential movement representations based on correlated neuronal activity. *Exp Brain Res*. 2003;149:478-486. doi:10.1007/s00221-003-1385-9
12. Daie K, Svoboda K, Druckmann S. Targeted photostimulation uncovers circuit motifs supporting short-term memory. *Nat Neurosci*. 2021;24(2):259-265. doi:10.1038/s41593-020-00776-3
13. Khanna P, Totten D, Novik L, Jeffrey Roberts, Morecraft RJ, Ganguly K. Low-frequency stimulation enhances ensemble co-firing and dexterity after stroke. *Cell*. 2021;184(4):912-930.e20. doi:10.1016/j.cell.2021.01.023
14. Ganguly K, Carmena JM. Emergence of a Stable Cortical Map for Neuroprosthetic Control. *PLOS Biol*. 2009;7(7):e1000153. doi:10.1371/journal.pbio.1000153
15. Peters AJ, Chen SX, Komiyama T. Emergence of reproducible spatiotemporal activity during motor learning. *Nature*. 2014;510(7504):263-267. doi:10.1038/nature13235
16. Rostami V, Rost T, Schmitt FJ, Albada SJ van, Riehle A, Nawrot MP. Spiking attractor model of motor cortex explains modulation of neural and behavioral variability by prior target information. Published online March 5, 2024:2020.02.27.968339. doi:10.1101/2020.02.27.968339
17. Guo L, Kondapavulur S, Lemke SM, Won SJ, Ganguly K. Coordinated increase of reliable cortical and striatal ensemble activations during recovery after stroke. *Cell Rep*. 2021;36(2):109370. doi:10.1016/j.celrep.2021.109370
18. Chang EF. Towards Large-Scale, Human-Based, Mesoscopic Neurotechnologies. *Neuron*. 2015;86(1):68-78. doi:10.1016/j.neuron.2015.03.037
19. Singh A. Oscillatory activity in the cortico-basal ganglia-thalamic neural circuits in Parkinson's disease. *Eur J Neurosci*. 2018;48(8):2869-2878. doi:10.1111/ejn.13853
20. Crone NE, Miglioretti DL, Gordon B, Lesser RP. Functional mapping of human sensorimotor cortex with electrocorticographic spectral analysis. II. Event-related synchronization in the gamma band. *Brain*. 1998;121(12):2301-2315. doi:10.1093/brain/121.12.2301
21. Fasano A, Mazzoni A, Falotico E. Reaching and Grasping Movements in Parkinson's Disease: A Review. *J Park Dis*. 2022;12(4):1083-1113. doi:10.3233/JPD-213082
22. Avanzino L, Pelosin E, Martino D, Abbruzzese G. Motor Timing Deficits in Sequential Movements in Parkinson Disease Are Related to Action Planning: A Motor Imagery Study. *PLOS ONE*. 2013;8(9):e75454. doi:10.1371/journal.pone.0075454
23. Ruitenberg MFL, Duthoo W, Santens P, Notebaert W, Abrahamse EL. Sequential movement skill in

Parkinson's disease: A state-of-the-art. *Cortex*. 2015;65:102-112. doi:10.1016/j.cortex.2015.01.005
24. Meissner SN, Krause V, Südmeyer M, Hartmann CJ, Pollok B. Pre-stimulus beta power modulation during motor sequence learning is reduced in 'Parkinson's disease. *NeuroImage Clin*. 2019;24:102057. doi:10.1016/j.nicl.2019.102057
25. Rockhill AP, Mantovani A, Stedelin B, Nerison CS, Raslan AM, Swann NC. Stereo-EEG recordings extend known distributions of canonical movement-related oscillations. *J Neural Eng*. 2023;20(1):016007. doi:10.1088/1741-2552/acae0a
26. Brown P. Oscillatory nature of human basal ganglia activity: Relationship to the pathophysiology of Parkinson's disease. *Mov Disord*. 2003;18(4):357-363. doi:10.1002/mds.10358
27. Hahn G, Ponce-Alvarez A, Deco G, Aertsen A, Kumar A. Portraits of communication in neuronal networks. *Nat Rev Neurosci*. 2019;20(2):117-127. doi:10.1038/s41583-018-0094-0
28. Mazzoni A, Whittingstall K, Brunel N, Logothetis NK, Panzeri S. Understanding the relationships between spike rate and delta/gamma frequency bands of LFPs and EEGs using a local cortical network model. *NeuroImage*. 2010;52(3):956-972. doi:10.1016/j.neuroimage.2009.12.040
29. Schroeder CE, Lakatos P. Low-frequency neuronal oscillations as instruments of sensory selection. *Trends Neurosci*. 2009;32(1):10.1016/j.tins.2008.09.012. doi:10.1016/j.tins.2008.09.012
30. Lakatos P, Karmos G, Mehta AD, Ulbert I, Schroeder CE. Entrainment of neuronal oscillations as a mechanism of attentional selection. *Science*. 2008;320(5872):110-113. doi:10.1126/science.1154735
31. Muller L, Chavane F, Reynolds J, Sejnowski TJ. Cortical travelling waves: mechanisms and computational principles. *Nat Rev Neurosci*. 2018;19(5):255-268. doi:10.1038/nrn.2018.20
32. Kaufman MT, Churchland MM, Ryu SI, Shenoy KV. Cortical activity in the null space: permitting preparation without movement. *Nat Neurosci*. 2014;17(3):440-448. doi:10.1038/nn.3643
33. Churchland MM, Shenoy KV. Preparatory activity and the expansive null-space. *Nat Rev Neurosci*. 2024;25(4):213-236. doi:10.1038/s41583-024-00796-z
34. Lemke SM, Ramanathan DS, Guo L, Won SJ, Ganguly K. Emergent modular neural control drives coordinated motor actions. *Nat Neurosci*. 2019;22(7):1122-1131. doi:10.1038/s41593-019-0407-2
35. Taylor JA, Ivry RB. Flexible Cognitive Strategies during Motor Learning. *PLOS Comput Biol*. 2011;7(3):e1001096. doi:10.1371/journal.pcbi.1001096
36. Wulf G. Attentional focus and motor learning: a review of 15 years. *Int Rev Sport Exerc Psychol*. 2013;6(1):77-104. doi:10.1080/1750984X.2012.723728
37. Song JH. The role of attention in motor control and learning. *Curr Opin Psychol*. 2019;29:261-265. doi:10.1016/j.copsyc.2019.08.002
38. Clark D, Ivry RB. Multiple systems for motor skill learning. *Wiley Interdiscip Rev Cogn Sci*. 2010;1(4):461-467. doi:https://doi.org/10.1002/wcs.56
39. Serrien DJ, Ivry RB, Swinnen SP. The missing link between action and cognition. *Prog Neurobiol*. 2007;82(2):95-107. doi:10.1016/j.pneurobio.2007.02.003
40. Doyon J, Benali H. Reorganization and plasticity in the adult brain during learning of motor skills. *Curr Opin Neurobiol*. 2005;15(2):161-167. doi:10.1016/j.conb.2005.03.004
41. Pinsard B, Boutin A, Gabitov E, Lungu O, Benali H, Doyon J. Consolidation alters motor sequence-specific distributed representations. *eLife*. 2019;8. doi:10.7554/eLife.39324
42. Goetz CG, Tilley BC, Shaftman SR, et al. Movement Disorder Society-sponsored revision of the Unified Parkinson's Disease Rating Scale (MDS-UPDRS): Scale presentation and clinimetric testing results. *Mov Disord*. 2008;23(15):2129-2170. doi:10.1002/mds.22340
43. VanRullen R. How to Evaluate Phase Differences between Trial Groups in Ongoing Electrophysiological Signals. *Front Neurosci*. 2016;10:426. doi:10.3389/fnins.2016.00426
44. Saleh M, Reimer J, Penn R, Ojakangas CL, Hatsopoulos NG. Fast and Slow Oscillations in Human Primary Motor Cortex Predict Oncoming Behaviorally Relevant Cues. *Neuron*. 2010;65(4):461-471. doi:10.1016/j.neuron.2010.02.001
45. Hamel-Thibault A, Thénault F, Whittingstall K, Bernier PM. Delta-Band Oscillations in Motor Regions Predict Hand Selection for Reaching. *Cereb Cortex*. 2018;28(2):574-584. doi:10.1093/cercor/bhw392
46. Lachaux JP, Rodriguez E, Martinerie J, Varela FJ. Measuring phase synchrony in brain signals. *Hum Brain Mapp*. 1999;8(4):194-208. doi:10.1002/(SICI)1097-0193(1999)8:4<194::AID-HBM4>3.0.CO;2-C
47. Vinck M, van Wingerden M, Womelsdorf T, Fries P, Pennartz CMA. The pairwise phase consistency: A bias-free measure of rhythmic neuronal synchronization. *NeuroImage*. 2010;51(1):112-122. doi:10.1016/j.neuroimage.2010.01.073

48. Nolte G, Ziehe A, Nikulin VV, et al. Robustly Estimating the Flow Direction of Information in Complex Physical Systems. *Phys Rev Lett*. 2008;100(23):234101. doi:10.1103/PhysRevLett.100.234101
49. Ramanathan DS, Guo L, Gulati T, et al. Low-frequency cortical activity is a neuromodulatory target that tracks recovery after stroke. *Nat Med*. 2018;24(8):1257-1267. doi:10.1038/s41591-018-0058-y
50. Muralidharan V, Aron AR. Behavioral Induction of a High Beta State in Sensorimotor Cortex Leads to Movement Slowing. *J Cogn Neurosci*. 2021;33(7):1311-1328. doi:10.1162/jocn_a_01717
51. Torrecillos F, Tinkhauser G, Fischer P, et al. Modulation of Beta Bursts in the Subthalamic Nucleus Predicts Motor Performance. *J Neurosci*. 2018;38(41):8905-8917. doi:10.1523/JNEUROSCI.1314-18.2018
52. Yin Z, Zhu G, Zhao B, et al. Local field potentials in Parkinson's disease: A frequency-based review. *Neurobiol Dis*. 2021;155:105372. doi:10.1016/j.nbd.2021.105372
53. Pascual-Leone A, Valls-Solé J, Brasil-Neto JP, Cohen LG, Hallett M. Akinesia in Parkinson's disease. I. Shortening of simple reaction time with focal, single-pulse transcranial magnetic stimulation. *Neurology*. 1994;44(5):884-884. doi:10.1212/WNL.44.5.884
54. Herrojo Ruiz M, Brücke C, Nikulin VV, Schneider GH, Kühn AA. Beta-band amplitude oscillations in the human internal globus pallidus support the encoding of sequence boundaries during initial sensorimotor sequence learning. *NeuroImage*. 2014;85:779-793. doi:10.1016/j.neuroimage.2013.05.085
55. Herrojo Ruiz M, Rusconi M, Brücke C, Haynes JD, Schönecker T, Kühn AA. Encoding of sequence boundaries in the subthalamic nucleus of patients with Parkinson's disease. *Brain J Neurol*. 2014;137(Pt 10):2715-2730. doi:10.1093/brain/awu191
56. Jenkinson N, Kühn AA, Brown P. Gamma oscillations in the human basal ganglia. *Exp Neurol*. 2013;245:72-76. doi:10.1016/j.expneurol.2012.07.005
57. Combrisson E, Perrone-Bertolotti M, Soto JL, et al. From intentions to actions: Neural oscillations encode motor processes through phase, amplitude and phase-amplitude coupling. *NeuroImage*. 2017;147:473-487. doi:10.1016/j.neuroimage.2016.11.042
58. Attaheri A, Choisdealbha ÁN, Di Liberto GM, et al. Delta- and theta-band cortical tracking and phase-amplitude coupling to sung speech by infants. *NeuroImage*. 2022;247:118698. doi:10.1016/j.neuroimage.2021.118698
59. Natraj N, Silversmith DB, Chang EF, Ganguly K. Compartmentalized dynamics within a common multi-area mesoscale manifold represent a repertoire of human hand movements. *Neuron*. 2022;110(1):154-174.e12. doi:10.1016/j.neuron.2021.10.002
60. Pal A, Pegwal N, Behari M, Sharma R. High delta and gamma EEG power in resting state characterise dementia in Parkinson's patients. *Biomark Neuropsychiatry*. 2020;3:100027. doi:10.1016/j.bionps.2020.100027
61. Ponsen MM, Stam CJ, Bosboom JLW, Berendse HW, Hillebrand A. A three dimensional anatomical view of oscillatory resting-state activity and functional connectivity in Parkinson's disease related dementia: An MEG study using atlas-based beamforming. *NeuroImage Clin*. 2013;2:95-102. doi:10.1016/j.nicl.2012.11.007
62. Rucco R, Lardone A, Liparoti M, et al. Brain Networks and Cognitive Impairment in Parkinson's Disease. *Brain Connect*. 2022;12(5):465-475. doi:10.1089/brain.2020.0985
63. Ray S, Crone NE, Niebur E, Franaszczuk PJ, Hsiao SS. Neural Correlates of High-Gamma Oscillations (60–200 Hz) in Macaque Local Field Potentials and Their Potential Implications in Electrocorticography. *J Neurosci*. 2008;28(45):11526-11536. doi:10.1523/JNEUROSCI.2848-08.2008
64. Doyon J. Motor sequence learning and movement disorders. *Curr Opin Neurol*. 2008;21(4):478-483. doi:10.1097/WCO.0b013e328304b6a3
65. Rusu SI, Pennartz CMA. Learning, memory and consolidation mechanisms for behavioral control in hierarchically organized cortico-basal ganglia systems. *Hippocampus*. 2020;30(1):73-98. doi:10.1002/hipo.23167
66. Caligiore D, Arbib MA, Miall RC, Baldassarre G. The super-learning hypothesis: Integrating learning processes across cortex, cerebellum and basal ganglia. *Neurosci Biobehav Rev*. 2019;100:19-34. doi:10.1016/j.neubiorev.2019.02.008
67. Simonyan K. Recent advances in understanding the role of the basal ganglia. *F1000Research*. 2019;8:F1000 Faculty Rev-122. doi:10.12688/f1000research.16524.1
68. Klaus A, Silva JA da, Costa RM. What, If, and When to Move: Basal Ganglia Circuits and Self-Paced Action Initiation. *Annu Rev Neurosci*. 2019;42(Volume 42, 2019):459-483. doi:10.1146/annurev-neuro-072116-031033

69. Balleine BW, Dezfouli A, Ito M, Doya K. Hierarchical control of goal-directed action in the cortical–basal ganglia network. *Curr Opin Behav Sci*. 2015;5:1-7. doi:10.1016/j.cobeha.2015.06.001
70. Milardi D, Quartarone A, Bramanti A, et al. The Cortico-Basal Ganglia-Cerebellar Network: Past, Present and Future Perspectives. *Front Syst Neurosci*. 2019;13. doi:10.3389/fnsys.2019.00061
71. Toni I, Rowe J, Stephan KE, Passingham RE. Changes of Cortico-striatal Effective Connectivity during Visuomotor Learning. *Cereb Cortex*. 2002;12(10):1040-1047. doi:10.1093/cercor/12.10.1040
72. Doyon J, Penhune V, Ungerleider LG. Distinct contribution of the cortico-striatal and cortico-cerebellar systems to motor skill learning. *Neuropsychologia*. 2003;41(3):252-262. doi:10.1016/S0028-3932(02)00158-6
73. Debas K, Carrier J, Barakat M, et al. Off-line consolidation of motor sequence learning results in greater integration within a cortico-striatal functional network. *NeuroImage*. 2014;99:50-58. doi:10.1016/j.neuroimage.2014.05.022
74. Wolff SBE, Ko R, Ölveczky BP. Distinct roles for motor cortical and thalamic inputs to striatum during motor skill learning and execution. *Sci Adv*. 2022;8(8):eabk0231. doi:10.1126/sciadv.abk0231
75. Kawai R, Markman T, Poddar R, et al. Motor Cortex Is Required for Learning but Not for Executing a Motor Skill. *Neuron*. 2015;86(3):800-812. doi:10.1016/j.neuron.2015.03.024
76. Murray JM, Escola GS. Learning multiple variable-speed sequences in striatum via cortical tutoring. Frank MJ, ed. *eLife*. 2017;6:e26084. doi:10.7554/eLife.26084
77. Sun H, Blakely TM, Darvas F, et al. Sequential activation of premotor, primary somatosensory and primary motor areas in humans during cued finger movements. *Clin Neurophysiol*. 2015;126(11):2150-2161. doi:10.1016/j.clinph.2015.01.005
78. Canavier CC. Phase-resetting as a tool of information transmission. *Curr Opin Neurobiol*. 2015;31:206-213. doi:10.1016/j.conb.2014.12.003
79. Harmony T. The functional significance of delta oscillations in cognitive processing. *Front Integr Neurosci*. 2013;7. doi:10.3389/fnint.2013.00083
80. Voloh B, Womelsdorf T. A Role of Phase-Resetting in Coordinating Large Scale Neural Networks During Attention and Goal-Directed Behavior. *Front Syst Neurosci*. 2016;10. doi:10.3389/fnsys.2016.00018
81. Miyachi S, Hikosaka O, Miyashita K, Kárádi Z, Rand MK. Differential roles of monkey striatum in learning of sequential hand movement. *Exp Brain Res*. 1997;115(1):1-5. doi:10.1007/PL00005669
82. Caproni S, Muti M, Principi M, et al. Complexity of Motor Sequences and Cortical Reorganization in Parkinson's Disease: A Functional MRI Study. *PLOS ONE*. 2013;8(6):e66834. doi:10.1371/journal.pone.0066834
83. Johansson ME, Toni I, Kessels RPC, Bloem BR, Helmich RC. Clinical severity in Parkinson's disease is determined by decline in cortical compensation. *Brain*. 2024;147(3):871-886. doi:10.1093/brain/awad325
84. Burciu RG, Vaillancourt DE. Imaging of Motor Cortex Physiology in Parkinson's Disease. *Mov Disord*. 2018;33(11):1688-1699. doi:10.1002/mds.102
85. Levy R, Ashby P, Hutchison WD, Lang AE, Lozano AM, Dostrovsky JO. Dependence of subthalamic nucleus oscillations on movement and dopamine in Parkinson's disease. *Brain*. 2002;125(6):1196-1209. doi:10.1093/brain/awf128
86. Zhuang P, Hallett M, Meng D, Zhang Y, Li Y. Characteristics of oscillatory activity in the globus pallidus internus in patients with Parkinson's disease (P1.8-028). *Neurology*. 2019;92(15 Supplement). doi:10.1212/WNL.92.15_supplement.P1.8-028
87. Whalen TC, Willard AM, Rubin JE, Gittis AH. Delta oscillations are a robust biomarker of dopamine depletion severity and motor dysfunction in awake mice. *J Neurophysiol*. 2020;124(2):312-329. doi:10.1152/jn.00158.2020
88. Tosin MHS, Stebbins GT, Comella C, Patterson CG, Hall DA, SPARX Study Group. Does MDS-UPDRS Provide Greater Sensitivity to Mild Disease than UPDRS in De Novo Parkinson's Disease? *Mov Disord Clin Pract*. 2021;8(7):1092-1099. doi:10.1002/mdc3.13329
89. Whittingstall K, Logothetis NK. Frequency-band coupling in surface EEG reflects spiking activity in monkey visual cortex. *Neuron*. 2009;64(2):281-289. doi:10.1016/j.neuron.2009.08.016
90. Wyart V, de Gardelle V, Scholl J, Summerfield C. Rhythmic fluctuations in evidence accumulation during decision making in the human brain. *Neuron*. 2012;76(4):847-858. doi:10.1016/j.neuron.2012.09.015
91. Dann B, Michaels JA, Schaffelhofer S, Scherberger H. Uniting functional network topology and oscillations in the fronto-parietal single unit network of behaving primates. Stephan KE, ed. *eLife*. 2016;5:e15719. doi:10.7554/eLife.15719

92. Kleen JK, Testorf ME, Roberts DW, et al. Oscillation Phase Locking and Late ERP Components of Intracranial Hippocampal Recordings Correlate to Patient Performance in a Working Memory Task. *Front Hum Neurosci*. 2016;10. doi:10.3389/fnhum.2016.00287
93. Gaidica M, Hurst A, Cyr C, Leventhal DK. Interactions Between Motor Thalamic Field Potentials and Single-Unit Spiking Are Correlated With Behavior in Rats. *Front Neural Circuits*. 2020;14. doi:10.3389/fncir.2020.00052
94. Fleischer P, Abbasi A, Fealy AW, et al. Emergent Low-Frequency Activity in Cortico-Cerebellar Networks with Motor Skill Learning. *eNeuro*. 2023;10(2). doi:10.1523/ENEURO.0011-23.2023
95. Riddle J, McFerren A, Frohlich F. Causal role of cross-frequency coupling in distinct components of cognitive control. *Prog Neurobiol*. 2021;202:102033. doi:10.1016/j.pneurobio.2021.102033
96. Hall TM, de Carvalho F, Jackson A. A common structure underlies low-frequency cortical dynamics in movement, sleep, and sedation. *Neuron*. 2014;83(5):1185-1199. doi:10.1016/j.neuron.2014.07.022
97. Haberly LB, Shepherd GM. Current-density analysis of summed evoked potentials in opossum prepyriform cortex. *J Neurophysiol*. 1973;36(4):789-802. doi:10.1152/jn.1973.36.4.789
98. Rebert CS. Slow potential correlates of neuronal population responses in the cat's lateral geniculate nucleus. *Electroencephalogr Clin Neurophysiol*. 1973;35(5):511-515. doi:10.1016/0013-4694(73)90027-8
99. Mitzdorf U. Current source-density method and application in cat cerebral cortex: investigation of evoked potentials and EEG phenomena. *Physiol Rev*. 1985;65(1):37-100. doi:10.1152/physrev.1985.65.1.37
100. Parker A, Derrington A, Blakemore C, Logothetis NK. The neural basis of the blood–oxygen–level–dependent functional magnetic resonance imaging signal. *Philos Trans R Soc Lond B Biol Sci*. 2002;357(1424):1003-1037. doi:10.1098/rstb.2002.1114
101. Abrahamse E, Ruitenberg M, De Kleine E, Verwey WB. Control of automated behavior: insights from the discrete sequence production task. *Front Hum Neurosci*. 2013;7. doi:10.3389/fnhum.2013.00082

MAIN FIGURES

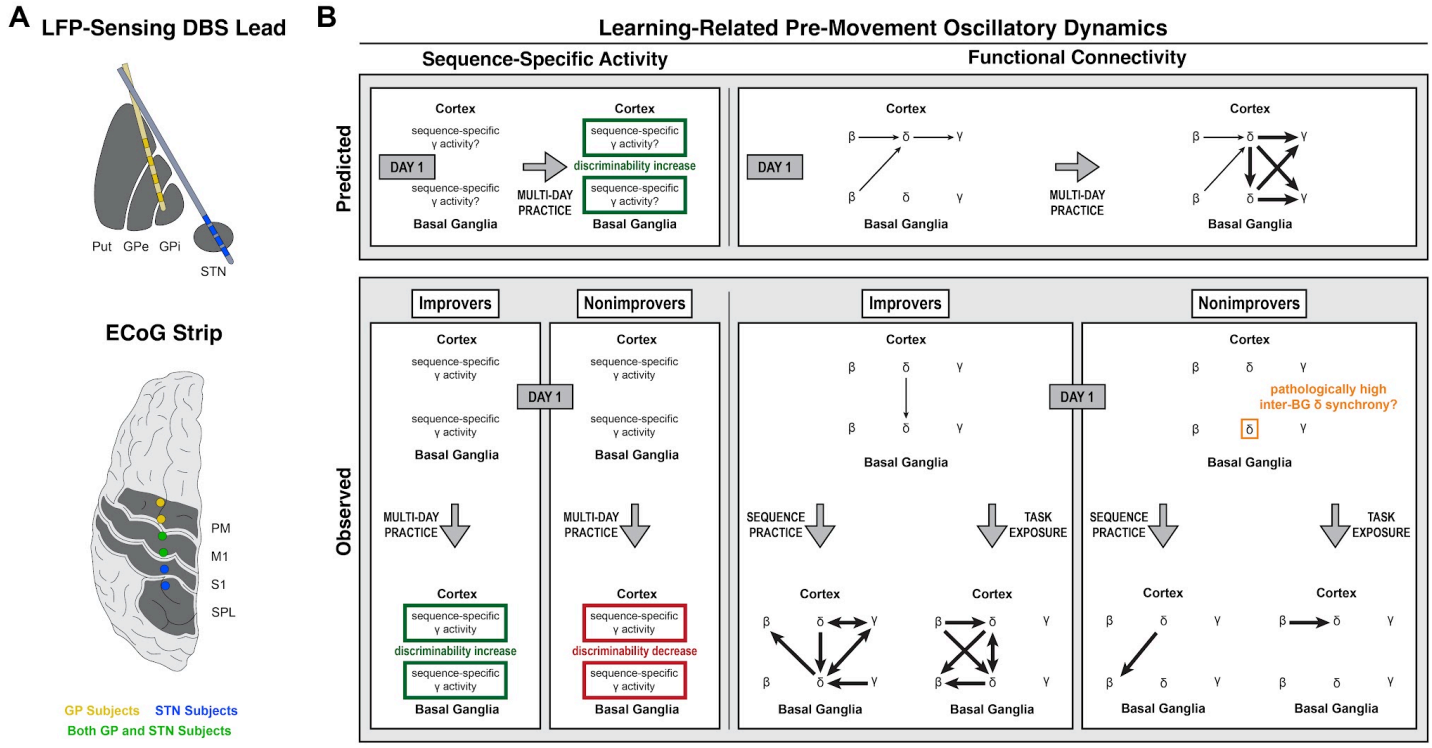

Figure 1. A model of learning-related cortico-basal ganglia activity during motor sequence initiation: predicted and observed. (**A**) Illustration of lead targeting for subject groups (LFP, local field potential; DBS, deep brain stimulation; ECoG, electrocorticography; Put, putamen; GPe, globus pallidus externus; GPi, globus pallidus internus; STN, subthalamic nucleus; PM, premotor cortex; M1, primary motor cortex; S1, primary somatosensory cortex; SPL, superior parietal lobule). (**B**) Diagram of predicted and observed learning-related changes in sequence-specific activity and functional connectivity prior to the onset of motor sequences over multiple days of practice. (Left, Top) For rapid, sequential finger movements, learning involves the optimization of preplanning for multiple sequence elements, potentially implemented by increased reliability of sequence-specific ensemble firing patterns in cortex and basal ganglia. This could be reflected by sequence-specific γ activity that becomes less noisy with practice, resulting in increased discriminability of neural activity related to different sequences. (Left, Bottom) Sequence-specific γ activity was present in all brain regions for all subjects. With practice, discriminability of sequence-specific γ activity increased in subjects who demonstrated performance improvement (improvers) but decreased in subjects who did not (nonimprovers). (Right, Top) Oscillatory network dynamics are thought to drive general motor initiation and may display learning-dependent changes that lead to increased reliability of ensemble activity patterns. One possibility is that network β desynchronization releases motor cortical excitability, reflected as δ phase modulation, which in turn facilitates activation of motor cortical ensembles to produce movement. With motor learning, increased cortico-basal ganglia δ synchrony facilitates enhanced ensemble recruitment. (Right, Bottom) As motor sequence learning overlaps with increasing familiarity with the experimental process, we disentangled the effects related to sequence learning from those related to task exposure. Improvers exhibited cortico-basal ganglia δ synchrony that, with sequence learning and task exposure, coincided with unique patterns of functional connectivity. In nonimprovers, basal ganglia δ was highly coherent and did not consistently respond to task events or coordinate with cortex. Very little learning-related functional connectivity was observed. Notably, no subjects demonstrated a consistent β→δ→γ cascade—possibly a reflection of PD-related neuropathophysiology.

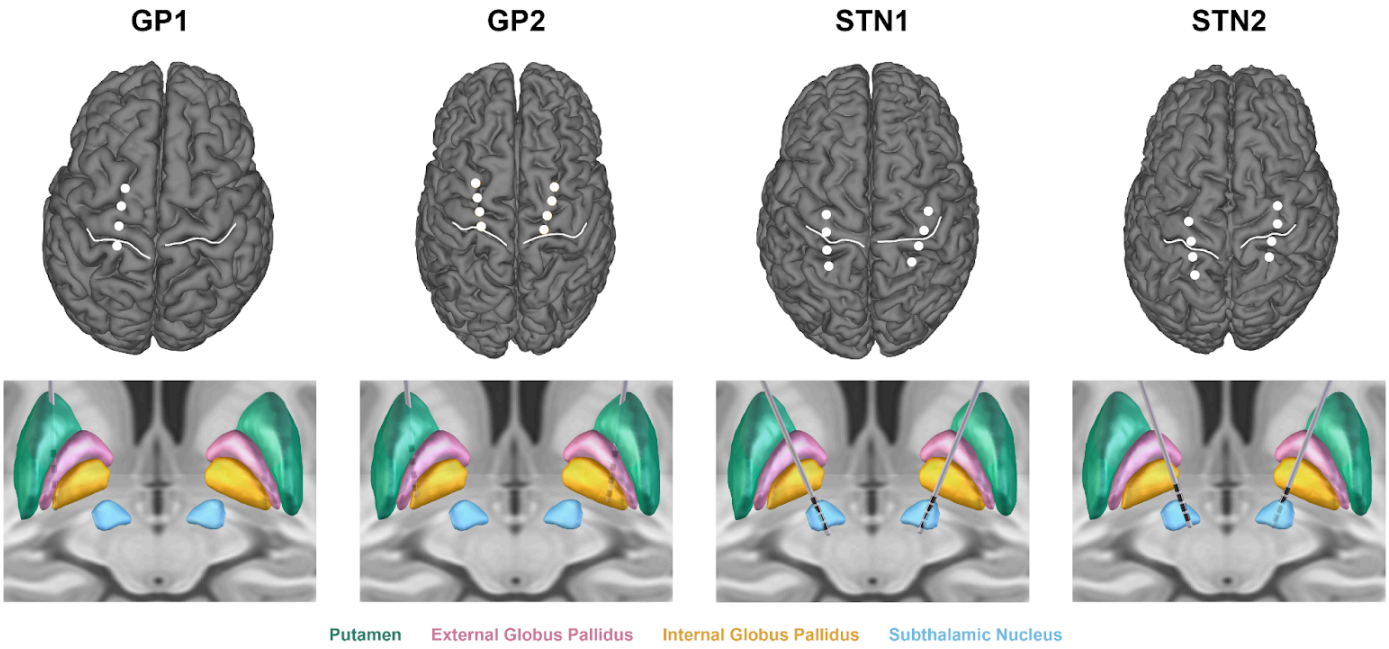

Figure 2. Cortical and subcortical lead reconstructions. (Top) Sensorimotor quadripolar electrocorticography strips, central sulci (white), and (Bottom) quadripolar deep brain stimulation leads localized within the basal ganglia.

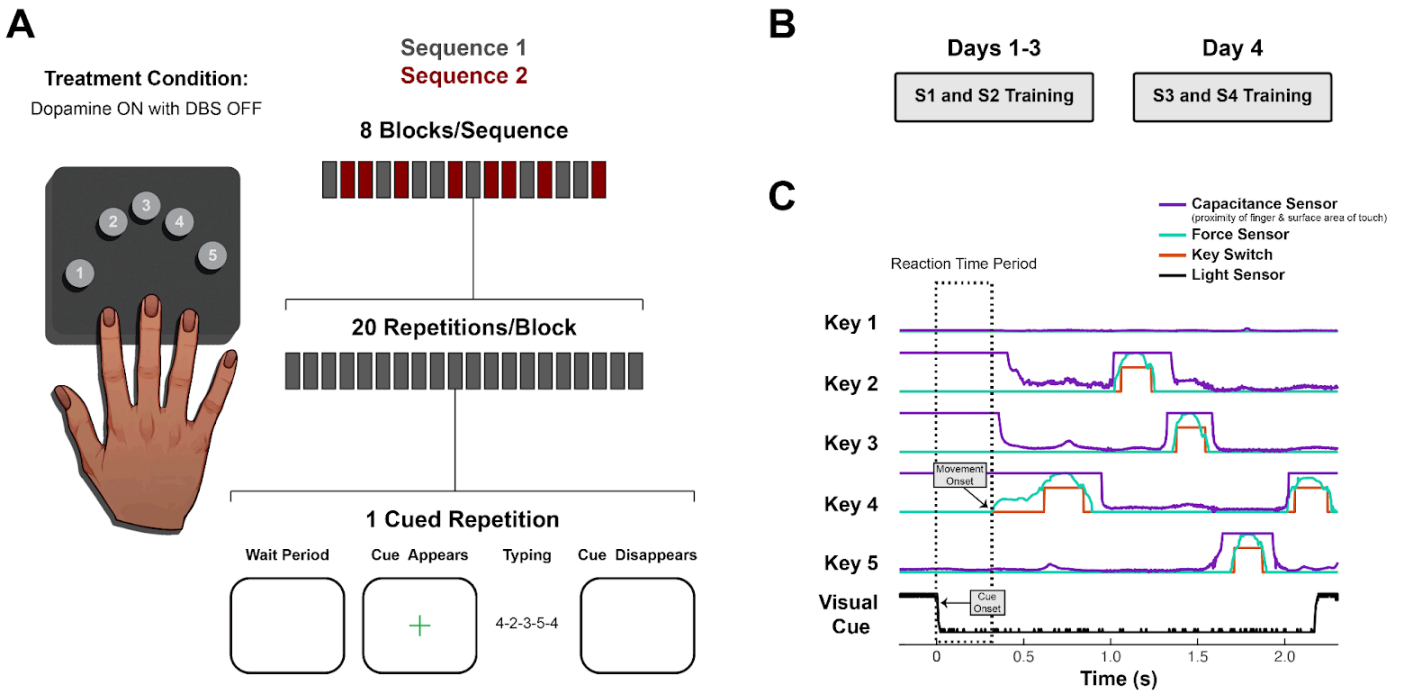

Figure 3. Experimental design and behavioral data collection. (**A**) On each day, subjects practiced typing two sequences. Interleaved practice blocks each contained 20 repetitions of visually cued sequence production for a single sequence. Subjects performed the task while on dopamine medication, and no DBS was delivered during the task or between days. (**B**) Days 1–3 employed novel Sequences 1 and 2 (S1 and S2), and Day 4 employed novel Sequences 3 and 4 (S3 and S4). (**C**) The reaction time period (dashed box) used for neural analysis is demonstrated in an example trial showing raw data from a custom behavioral setup used to capture finger movement (using capacitive proximity/touch sensors, force-sensitive resistors and mechanical key switches) and the visual cue (using a photodiode placed on the task computer screen). Capacitance sensors were calibrated to detect proximity changes of fingers hovering 0 to 2 cm above the keys (capacitance variation around low values). They could also detect changes in surface area of finger contact with the key associated with changes in force subthreshold for the force sensors (capacitance variation between low/mid-range and ceiling values). Thus, capacitance sensor readings were used for motor onset detection, except when motor onset began with a finger already in full contact with the key, in which case force sensor readings were used (as in the first keypress of this example trial).

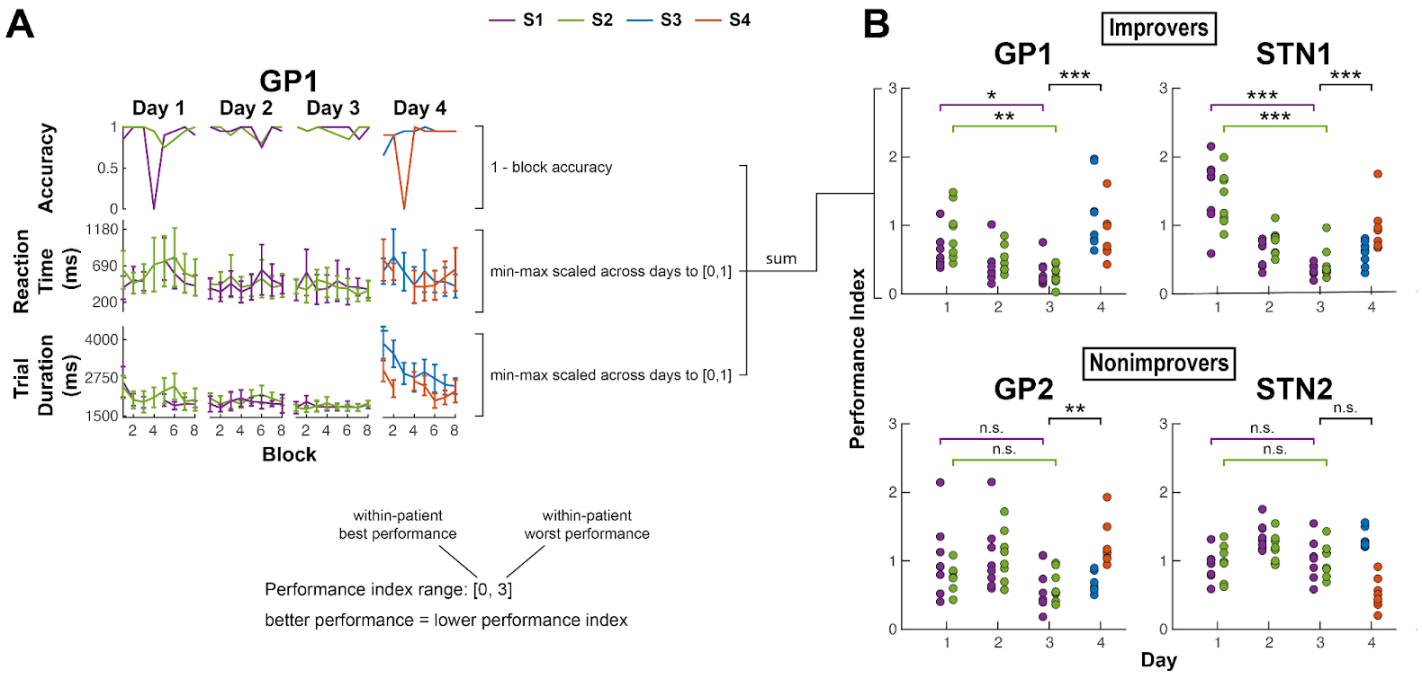

Figure 4. Behaviorally distinguishing improvers and nonimprovers. (A) Example calculation of block performance index (PI) from block average data. Each block performance index is the sum of block average error rate [1 – accuracy], reaction time [cue onset to movement onset] and trial duration [movement onset to offset]. Before combining into the performance index, block average trial duration and reaction time were each first within-subject min-max scaled across days to [0,1]. Error bars indicate ±*s*. **(B)** Block performance index for each subject. Comparison across Days 1 and 3 for each of S1 and S2 assessed within-sequence practice-driven performance changes. To help evaluate whether performance changes from Day 1 to Day 3 were at least in part related to sequence learning and not solely attributable to changing familiarity with the task and keypad, performance was also compared between pooled Day 3 sequences and pooled Day 4 sequences. Subjects were labeled improvers (ID ending in 1) only if their performance both improved from Day 1 to Day 3 and worsened when presented with novel sequences on Day 4 (For all comparisons: α=0.05, two-sided, two-sample *t*-test with unequal variance. Supplementary Data 4—1 *p*-Values). *p<0.05, **p<0.01, ***p<0.001.

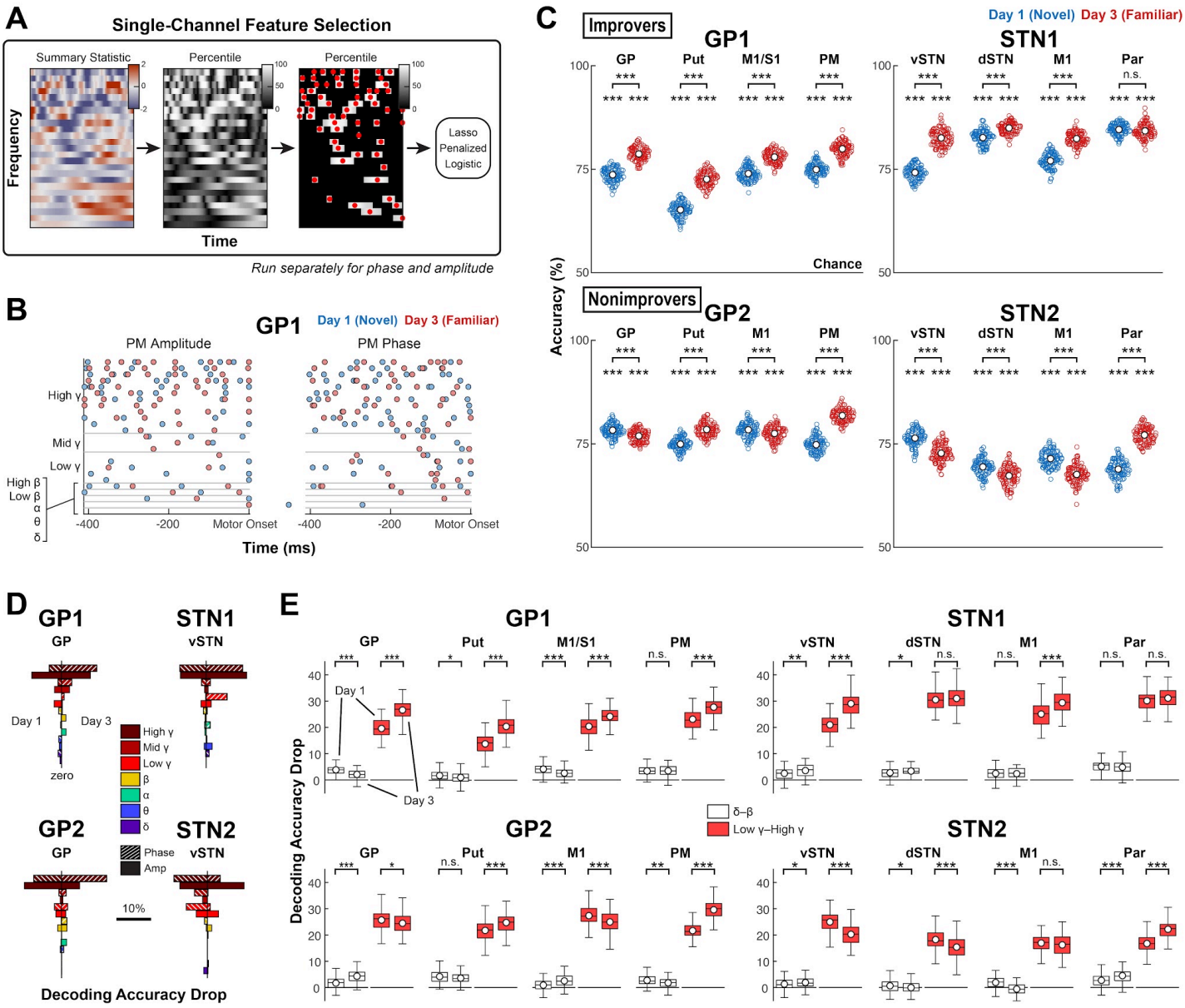

Figure 5. Pre-movement sequence-specific γ activity, present in all brain regions, demonstrates practice-driven increases and decreases in discriminability in improvers and nonimprovers, respectively. (**A**) Visualization of feature selection pipeline. Features were selected separately for each channel on each day in each subject. (Left) For selection of amplitude features, the S1 vs. S2 two-sided *t*-statistic was computed at each time-frequency point. (Middle) The *t*-statistic at each time-frequency point was recomputed for 10,000 permutations of trial labels to determine the percentile ranking of the test value at each time-frequency point relative to its null distribution. (Right) Time-frequency points falling below their respective 80th-percentile cutoffs were masked, and in each of the remaining time-frequency regions, the time point achieving the highest percentile was selected as an amplitude feature. This process was repeated for phase data, using phase opposition sum as the summary statistic. Each resulting phase feature was split into two features comprised of the cartesian phase coordinates. Classification utilized 10-fold 100-repeat lasso-penalized logistic classification. (**B**) Example selected features for Days 1 and 3 in GP1's PM. (**C**) Mean decoding accuracy per model after feature selection (Comparison to chance: α=0.05, one-sided, permutation testing with 1,000 resamples. Comparison across days: α=0.05, two-sided, permutation test with 10,000 resamples. Supplementary Data 5—1 *p*-Values). Empty circle reflects mean decoding accuracy across folds for one repeat; white circle reflects mean decoding accuracy across repeats. (**D**) Absolute decoding accuracy decreases for features grouped by canonical frequency band and signal property (amplitude or phase)—a subset of representative plots. (**E**) Absolute decoding accuracy decreases for features grouped by frequency into two groups: δ through β (0.5–30 Hz, phase and amplitude) and low γ through high γ (30–250 Hz, phase and amplitude) (Comparison across days: α=0.05, two-sided, permutation testing with 10,000 resamples. Supplementary Data 5—2 *p*-Values). White circle reflects mean; black horizontal line reflects median. Box edges correspond to 25th and 75th percentiles. Whiskers span the entire data range excluding outliers. Outliers were computed as $1.5 \cdot IQR$ away from the upper or lower quartile and are not shown. **p*<0.05, ***p*<0.01, ****p*<0.001.

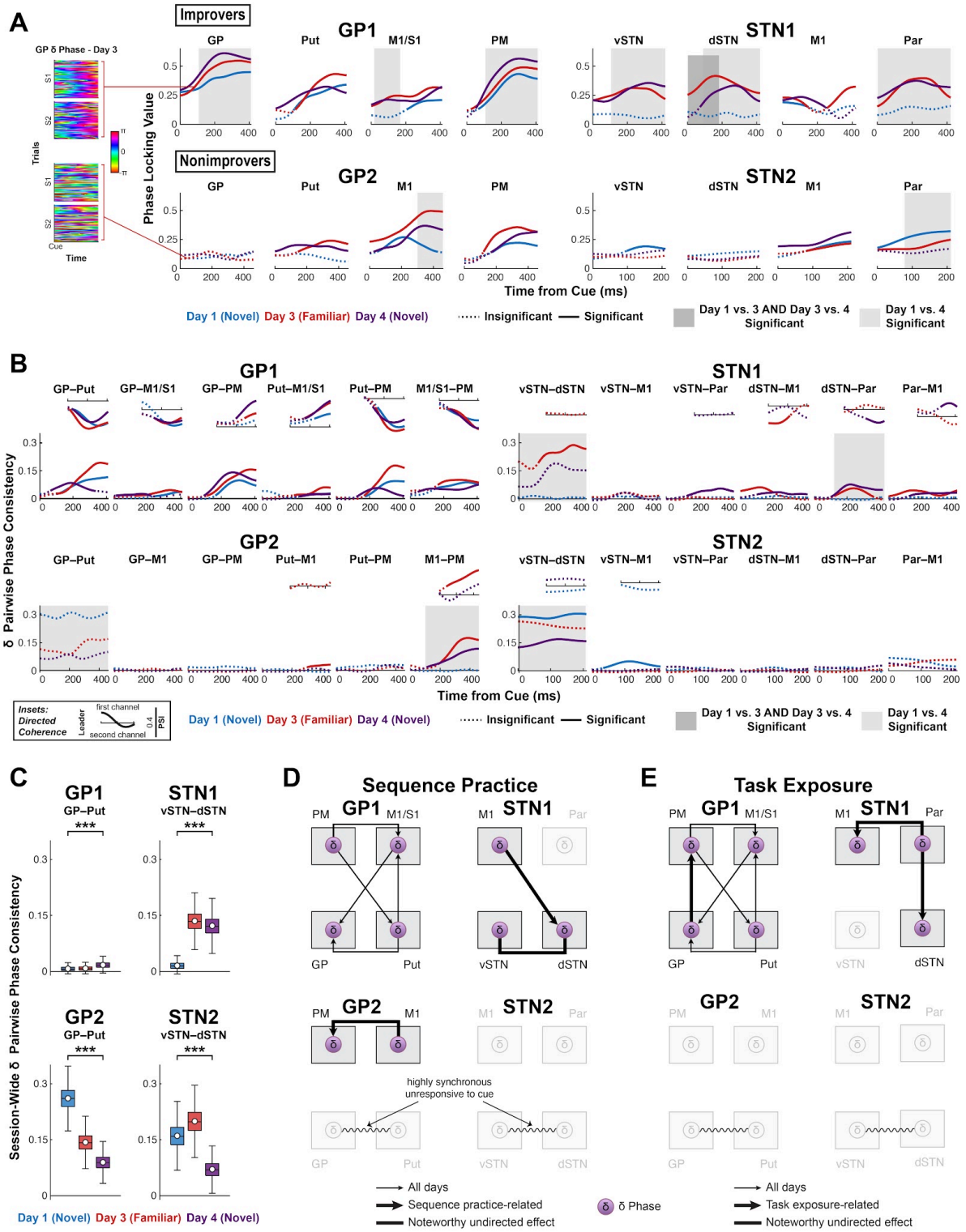

Figure 6. Improvement is associated with cortically-led network δ phase synchrony, to which sequence learning and task exposure add distinct effects, while lack of improvement is associated with highly synchronous BG δ. (**A**) (Left) All Day 3 single-trial δ phase time series after cue onset in the pallidum of GP1 and GP2. (Right) Phase locking value (PLV) after cue onset on Days 1, 3 and 4. Solid line indicates PLV significantly higher than chance (α=0.05, one-sided, cluster-based permutation test with 10,000 resamples. Supplementary Data 6—1 *p*-Values). Shaded box indicates significant difference in PLV between days (α=0.05, two-sided, cluster-based permutation with 10,000 resamples. Supplementary Data 6—1 *p*-Values). (**B**) Effects in δ synchrony. (Large plots) δ pairwise phase consistency (PPC, undirected measure) time series for all channel pairs. Solid line indicates PPC significantly higher than session-wide baseline, i.e., h_0=coherence aligned cue is the same as general coherence levels not aligned to cue (rather than h_0=no coherence) (α=0.05, one-sided, cluster-based permutation with 10,000 resamples. Supplementary Data 6—2 *p*-Values). Shaded box indicates significant difference in PPC between days (α=0.05, two-sided, cluster-based permutation with 10,000 resamples. Supplementary Data 6—2 *p*-Values). (Insets) Phase slope index (PSI, directed measure) for significant PPC time series. Solid line indicates significant PSI (h_0=no channel leads, α=0.05, two-sided, cluster-based permutation with 10,000 resamples. Supplementary Data 6—2 *p*-Values). (**C**) Session-wide baseline basal ganglia δ pairwise phase consistency averaged across time. Calculated by taking the null distribution of time series resampled from each session in (**B**) and averaging each null PPC sample across time. Change in session baseline across Days 1 and 4 was tested (α=0.05, two-sided, permutation testing with 10,000 resamples. Source Data 2). White circle reflects mean; black horizontal line reflects median. Box edges correspond to 25th and 75th percentiles. Whiskers span entire data range excluding outliers. Outliers were computed as 1.5·*IQR* away from the upper or lower quartile and are not shown. ***p<0.001. (**D**) Network diagrams illustrating sequence practice-related δ coherence effects. (**E**) Network diagrams illustrating task exposure-related δ coherence effects.

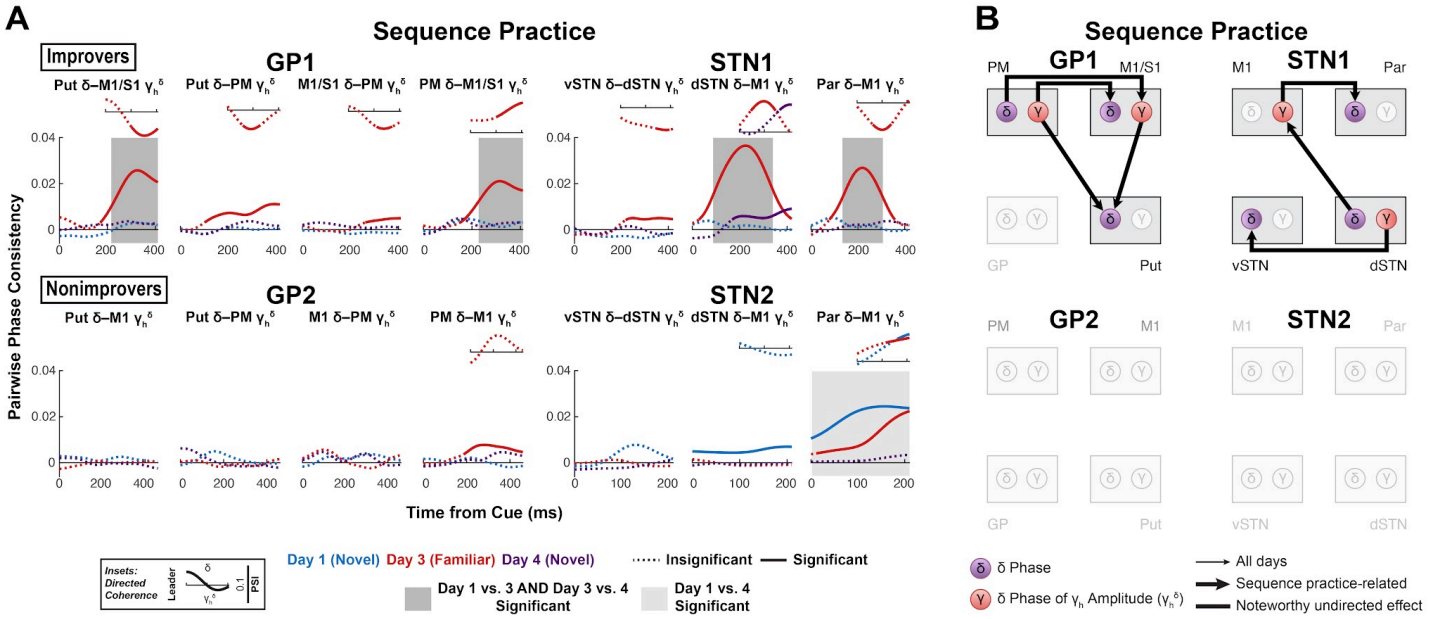

Figure 7. Sequence learning is associated with specific corticocortical, cortico-basal ganglia and inter-basal ganglia δ-γ couplings. (**A**) Sequence practice-related effects in interregional δ-γ_h^{δ} coherence. (Large plots) Pairwise phase consistency (PPC, undirected measure) was calculated between δ phase and the δ phase of the high γ amplitude envelope. Solid line indicates significant PPC (h_0=coherence is not higher than expected given the phase distribution, α=0.05, one-sided, cluster-based permutation with 10,000 resamples. Supplementary Data 7—1 *p*-Values). Shaded box indicates significant difference in PPC between days (α=0.05, two-sided, cluster-based permutation with 10,000 resamples. Supplementary Data 7—1 *p*-Values). (Insets) Phase slope index (PSI, directed measure) for significant PPC time series. Solid line indicates significant PSI (h_0=no channel leads, α=0.05, two-sided, cluster-based permutation with 10,000 resamples. Supplementary Data 7—1 *p*-Values). (**B**) Network diagrams illustrating sequence practice-related δ-γ_h^{δ} effects.

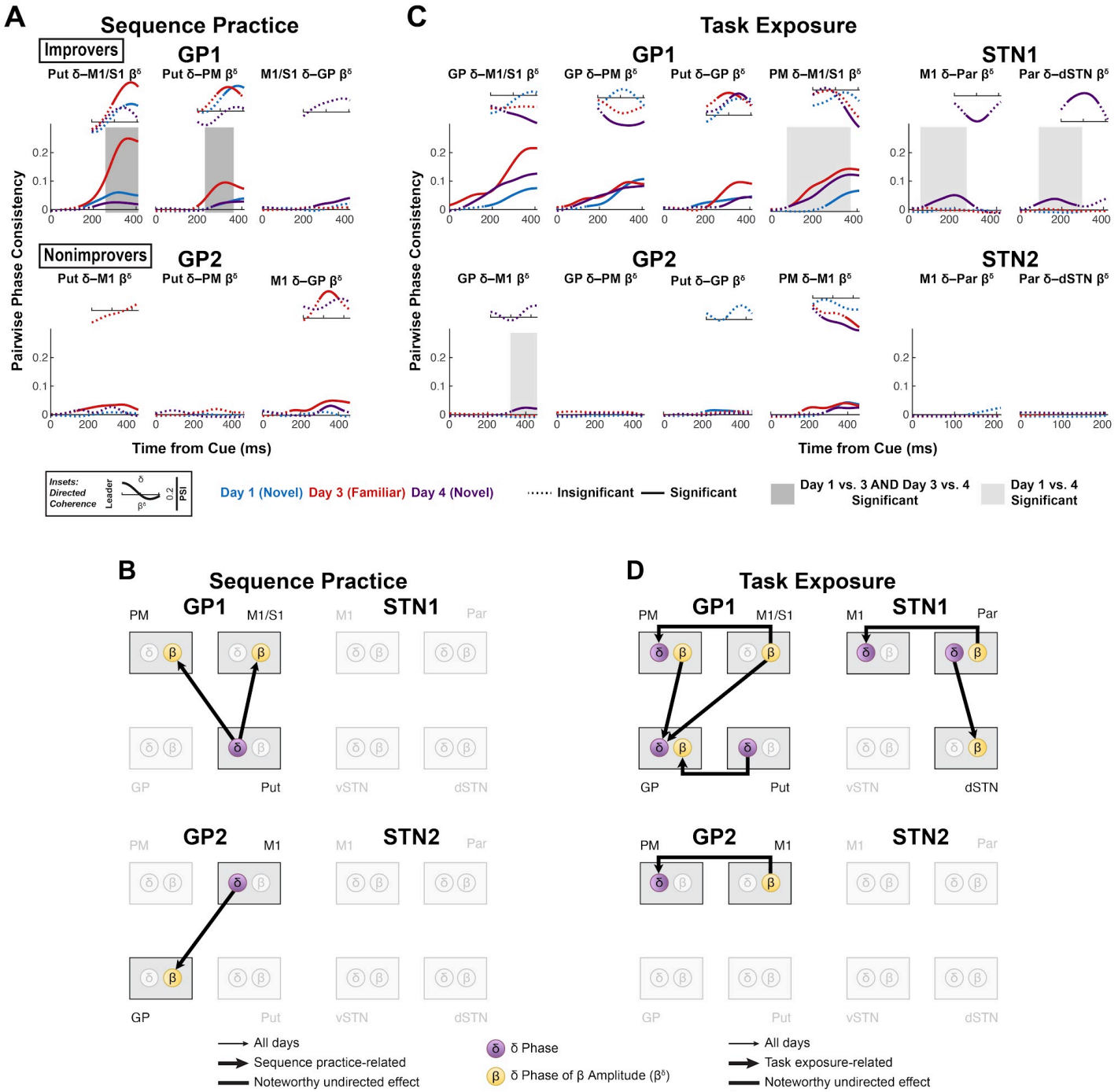

Figure 8. Striatocortical δ-β coupling increases with sequence learning; task exposure brings a range of δ-β couplings in improvers, mostly absent in nonimprovers. (**A**) Sequence practice-related effects in interregional δ-β^{δ} coherence. (Large plots) Pairwise phase consistency (PPC, undirected measure) was calculated between δ phase and the δ phase of the β amplitude envelope. Solid line indicates significant PPC (h_0=coherence is not higher than expected given the phase distribution, α=0.05, one-sided, cluster-based permutation with 10,000 resamples. Supplementary Data 8—1 *p*-Values). Shaded box indicates significant difference in PPC between days (α=0.05, two-sided, cluster-based permutation with 10,000 resamples. Supplementary Data 8—1 *p*-Values). (Insets) Phase slope index (PSI, directed measure) for significant PPC time series. Solid line indicates significant PSI (h_0=no channel leads, α=0.05, two-sided, cluster-based permutation with 10,000 resamples. Supplementary Data 8—1 *p*-Values). (**B**) Network diagrams illustrating sequence practice-related δ-β^{δ} effects. (**C**) Task exposure-related effects in interregional δ-β^{δ} coherence. Visualization and statistics identical to (**A**) (Supplementary Data 8—2 *p*-Values). (**D**) Network diagrams illustrating task exposure-related δ-β^{δ} effects.

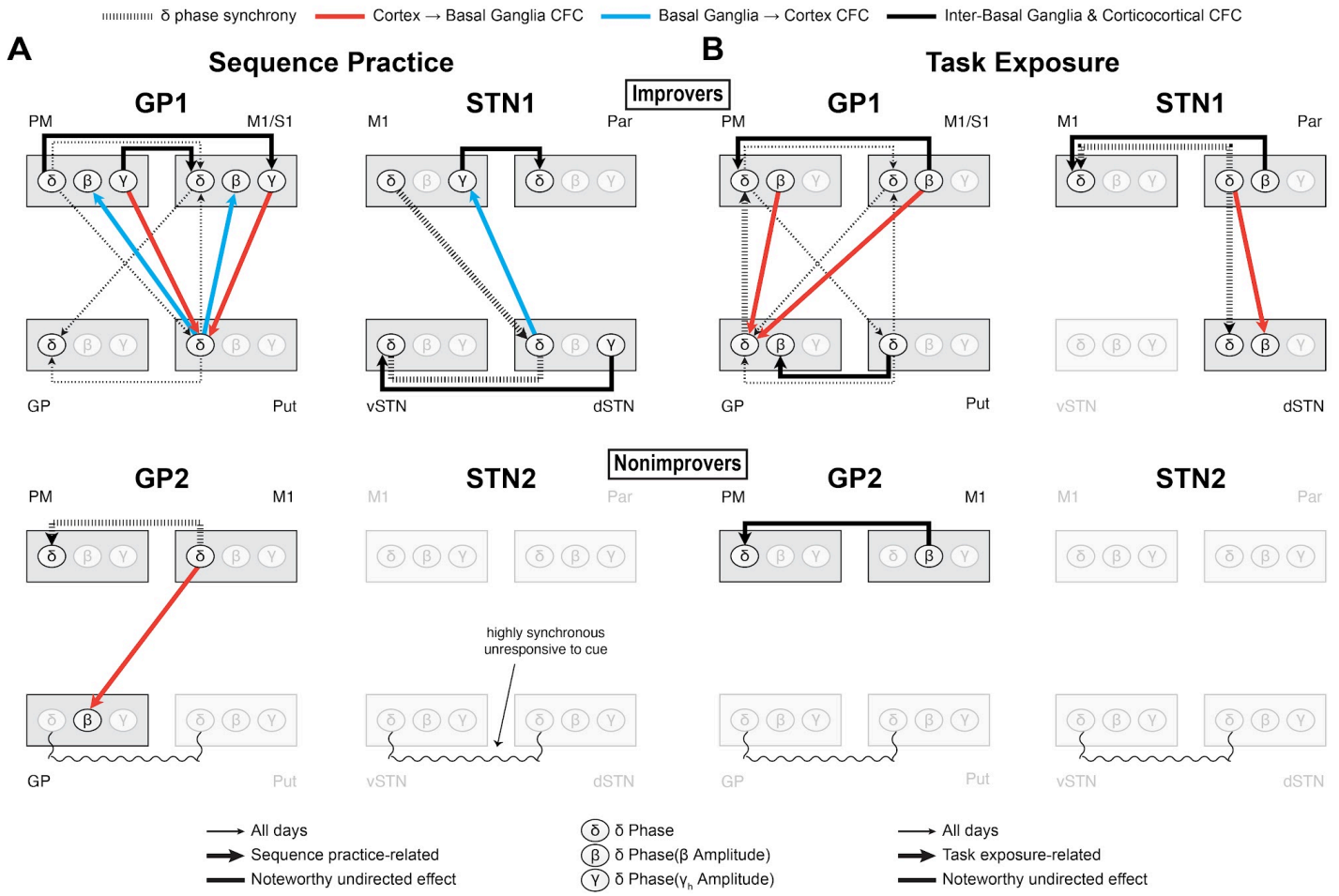

Figure 9. A learning-dependent hierarchical functional network architecture for sequence initiation reflects the unique roles of different brain regions in the cortico-basal ganglia network within a framework of coordinated network δ. Composite diagrams of interregional effects associated with (**A**) sequence practice and (**B**) task exposure. Notably, no directed δ-β^{δ} or δ-γ_h^{δ} interregional couplings were associated with general sequence initiation across days, and cross-frequency coupling (CFC) instead developed with sequence practice or task exposure. Furthermore, only brain regions that demonstrated δ phase alignment to cue and synchronized with motor cortical δ contributed δ to any learning-related interregional $\delta \rightarrow \beta^{\delta}$ or $\delta \rightarrow \gamma_h^{\delta}$ coupling. In improvers, sequence learning and task exposure brought different CFC patterns and changes to network δ dynamics, though sequence learning and task exposure were linked by a common framework of cortically-led network δ synchrony. Almost all observed communication between cortex and basal ganglia in improvers involved basal ganglia δ. Nevertheless, for each type of communication, the presence and direction of coupling depended on the involved brain regions, indicative of their unique roles. In nonimprovers, highly synchronized basal ganglia δ coincided with minimal functional connectivity in the assessed frequency bands.

SUPPLEMENTARY FIGURES

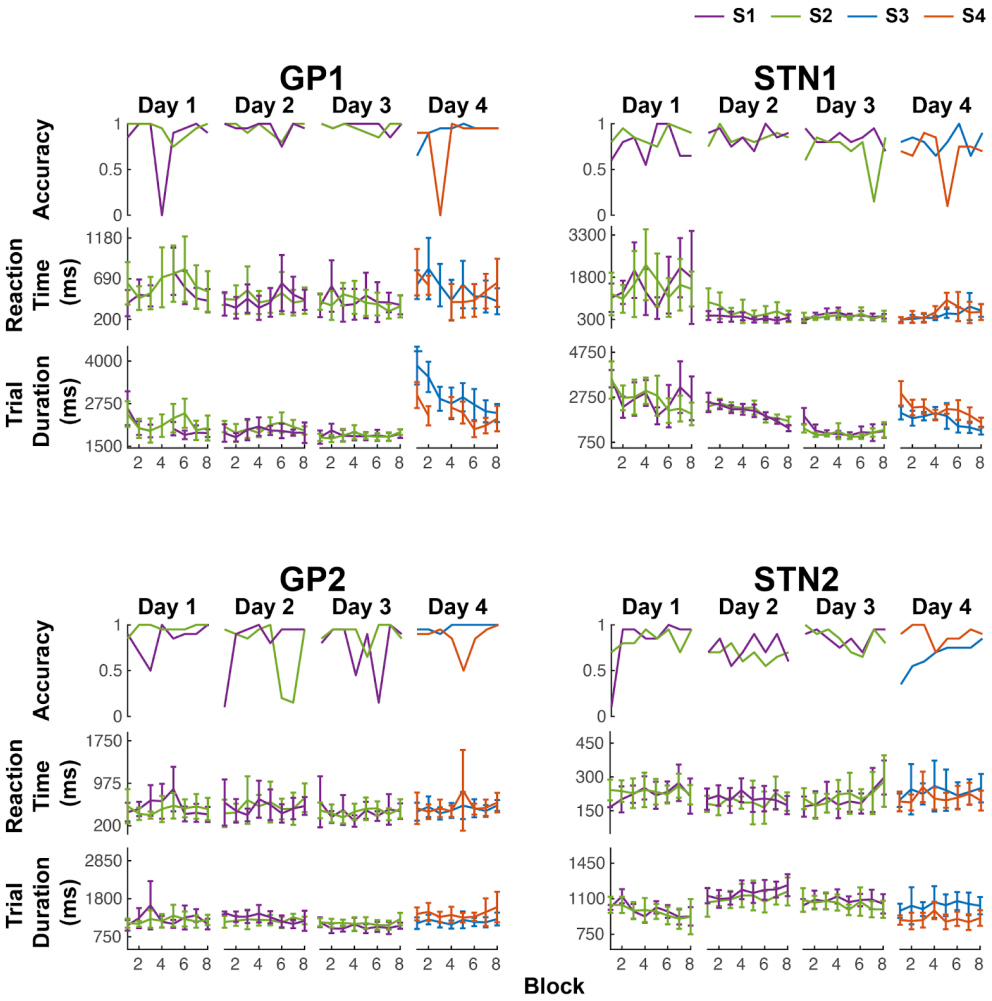

Figure 4–figure supplement 1. Block average performance data. Per subject: (Top) block average accuracy, (Middle) block average reaction time [cue onset to movement onset], (Bottom) block average trial duration [movement onset to offset]. Error bars indicate ±*s*.

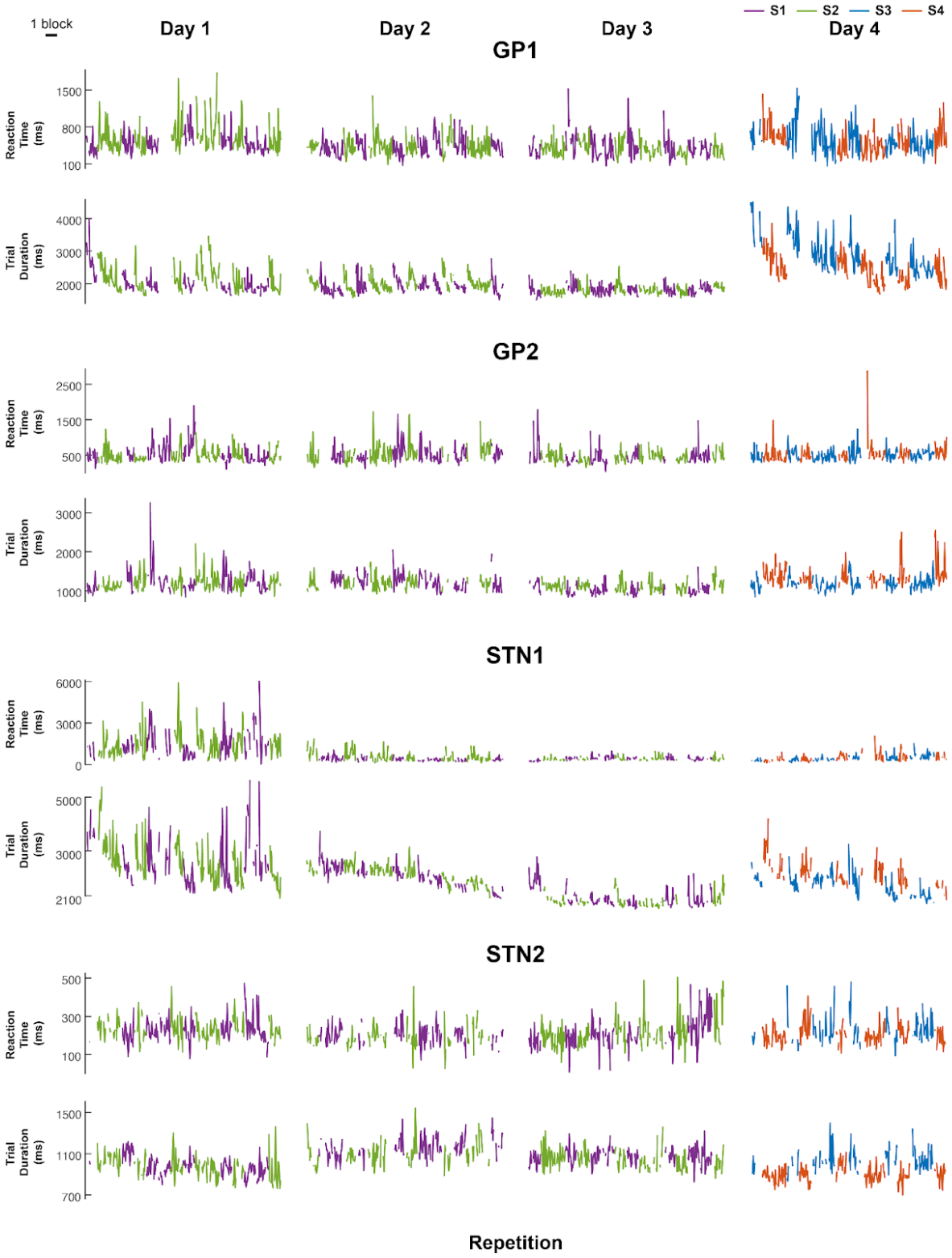

Figure 4–figure supplement 2. Single-trial performance data. Single-trial reaction time and trial duration for all fully correct trials.

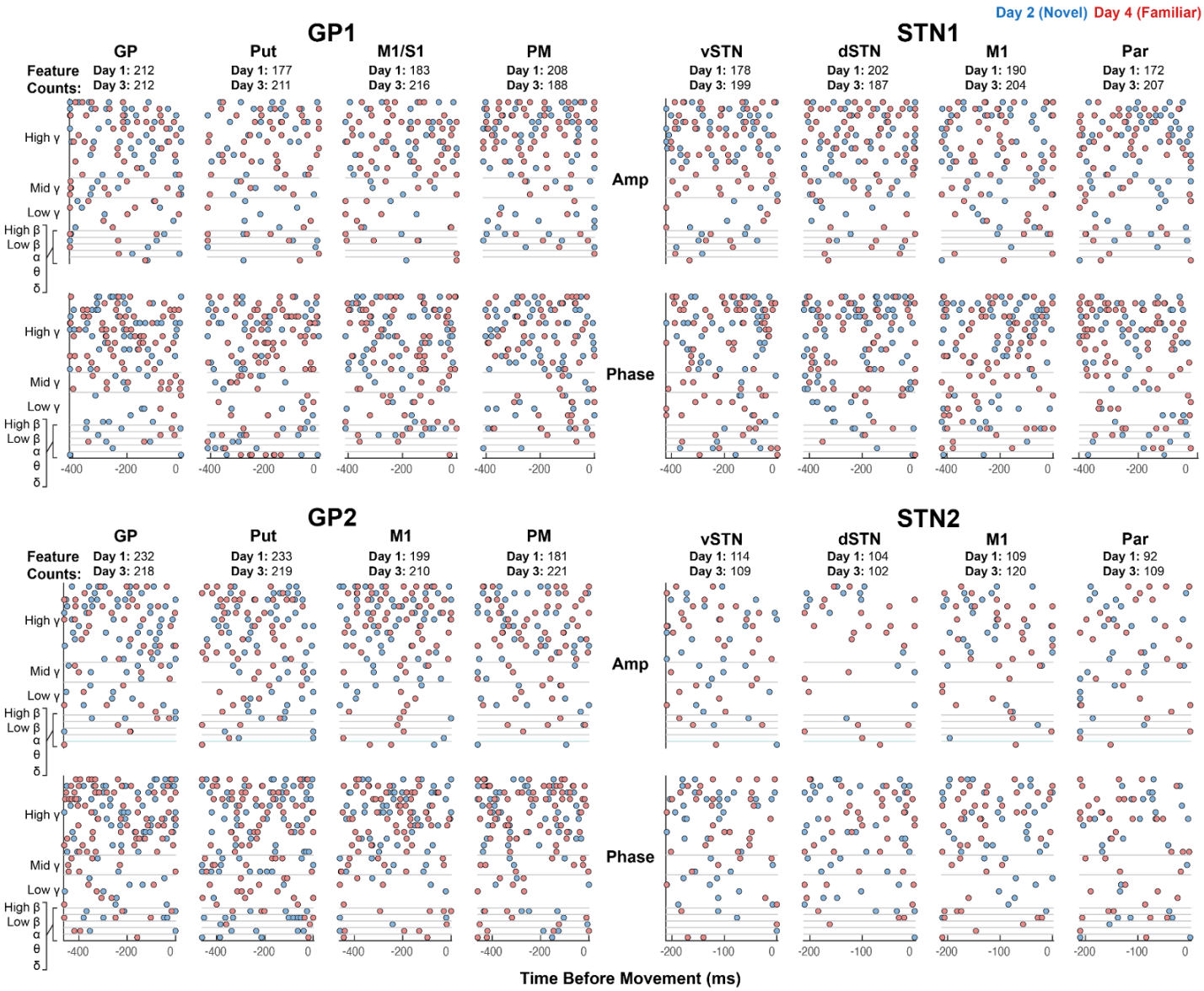

Figure 5–figure supplement 1. Selected features. Features were selected separately for each model. Total feature count per model (i.e., per subject per channel per day) prior to lasso regularization is shown above each channel's amplitude and phase feature plots. ***Feature counts are based on each design matrix and thus include a feature for both the sin(phase) and the cos(phase) of each selected phase time-frequency point.*** As a larger number of phase than amplitude time-frequency points tended to reach the 80th percentile cutoff for feature selection, the indicated total feature counts are at least 50% higher than the number of initially selected time-frequency points.

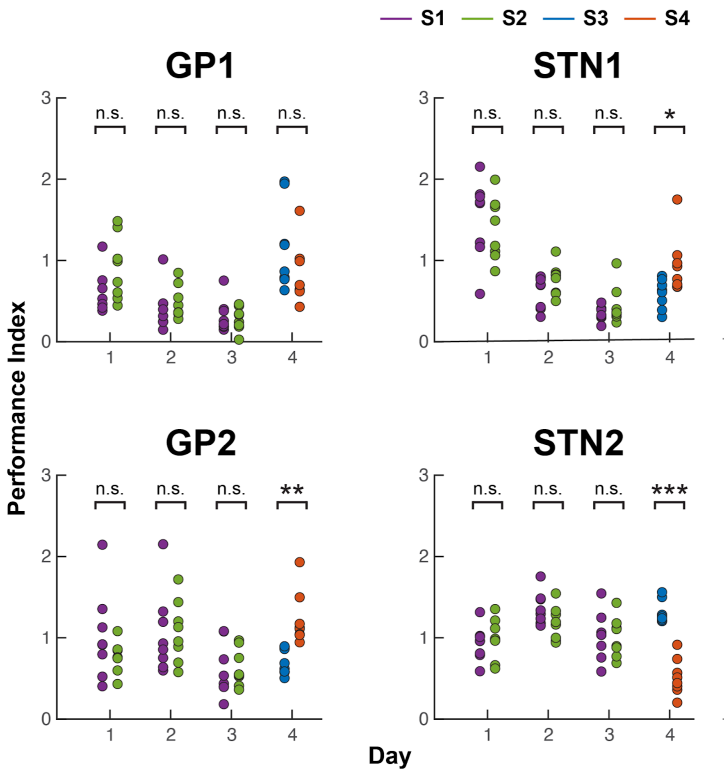

Figure 5–figure supplement 2. On Days 1–3, overall sequence performance was comparable between S1 and S2. Across-sequence comparison of performance within each day assessed differences in overall performance level (α=0.05, two-sided, two-sample t-test with unequal variance. Supplementary Data 5—3 *p*-Values). *p<0.05, **p<0.01, ***p<0.001.

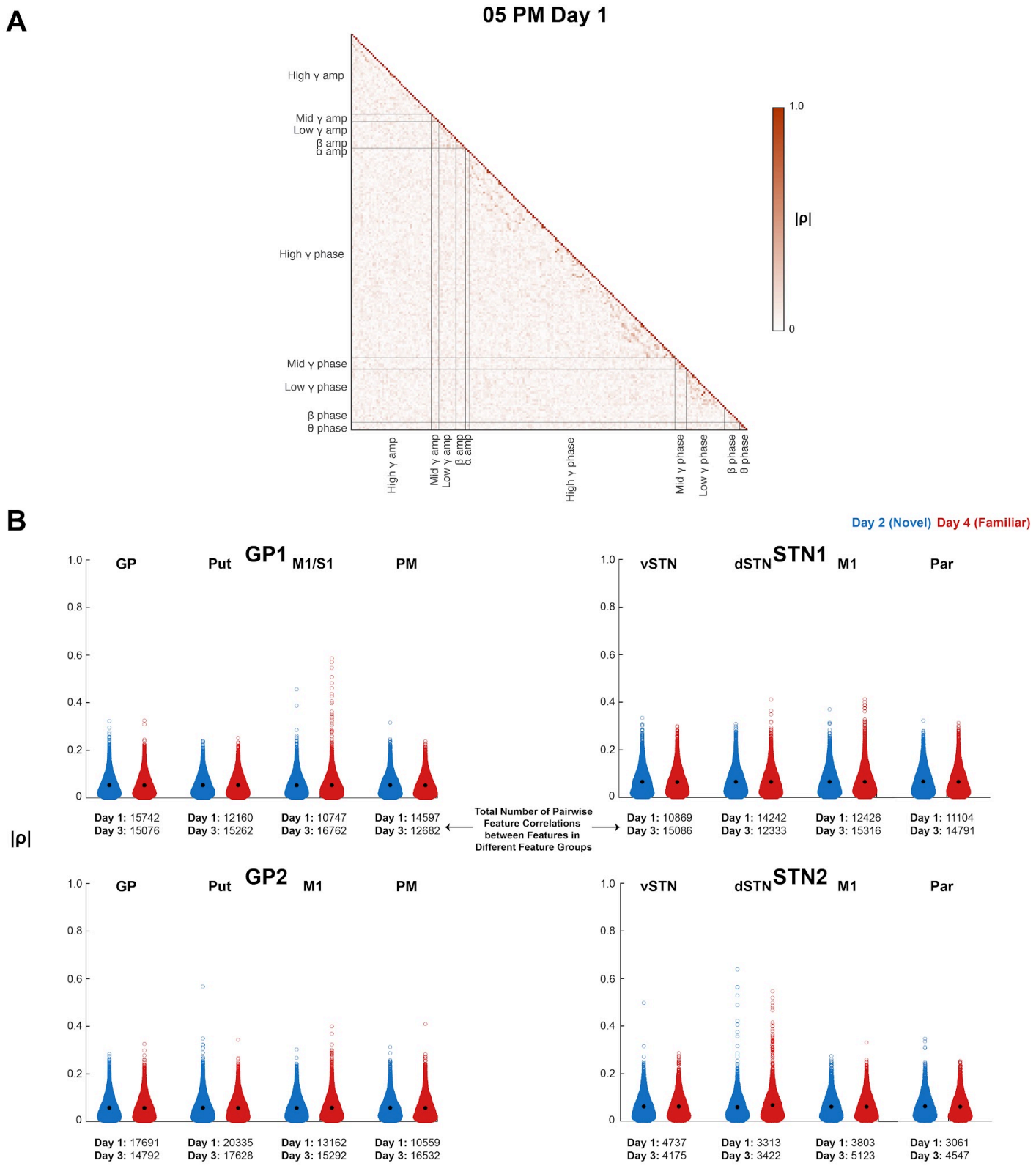

Figure 5–figure supplement 3. Correlations between features after grouping by canonical frequency band and signal property. (**A**) Example feature correlation matrix for a single model, where light gray lines separate feature groups. (**B**) For each model, a swarm plot of all possible feature correlations between features in different groups. Features were grouped by canonical frequency band and also by signal property, i.e., δ phase features were grouped separately from δ amplitude features, as well as from all other canonical frequency bands. Total number of feature correlations between features in different feature groups for a given model is shown below corresponding swarm plots.

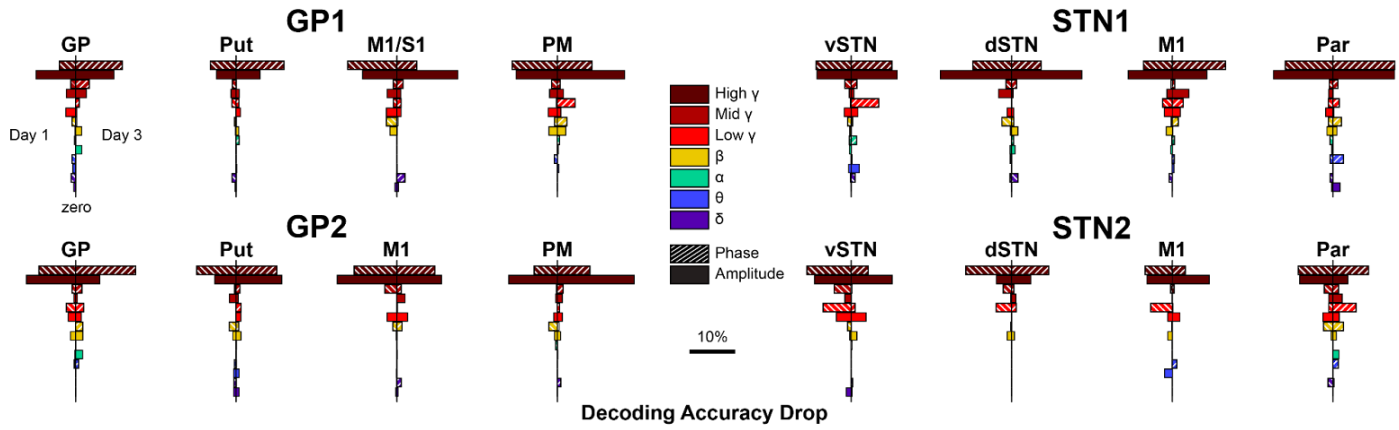

Figure 5–figure supplement 4. Absolute decoding accuracy decreases for features grouped by canonical frequency band and signal property.

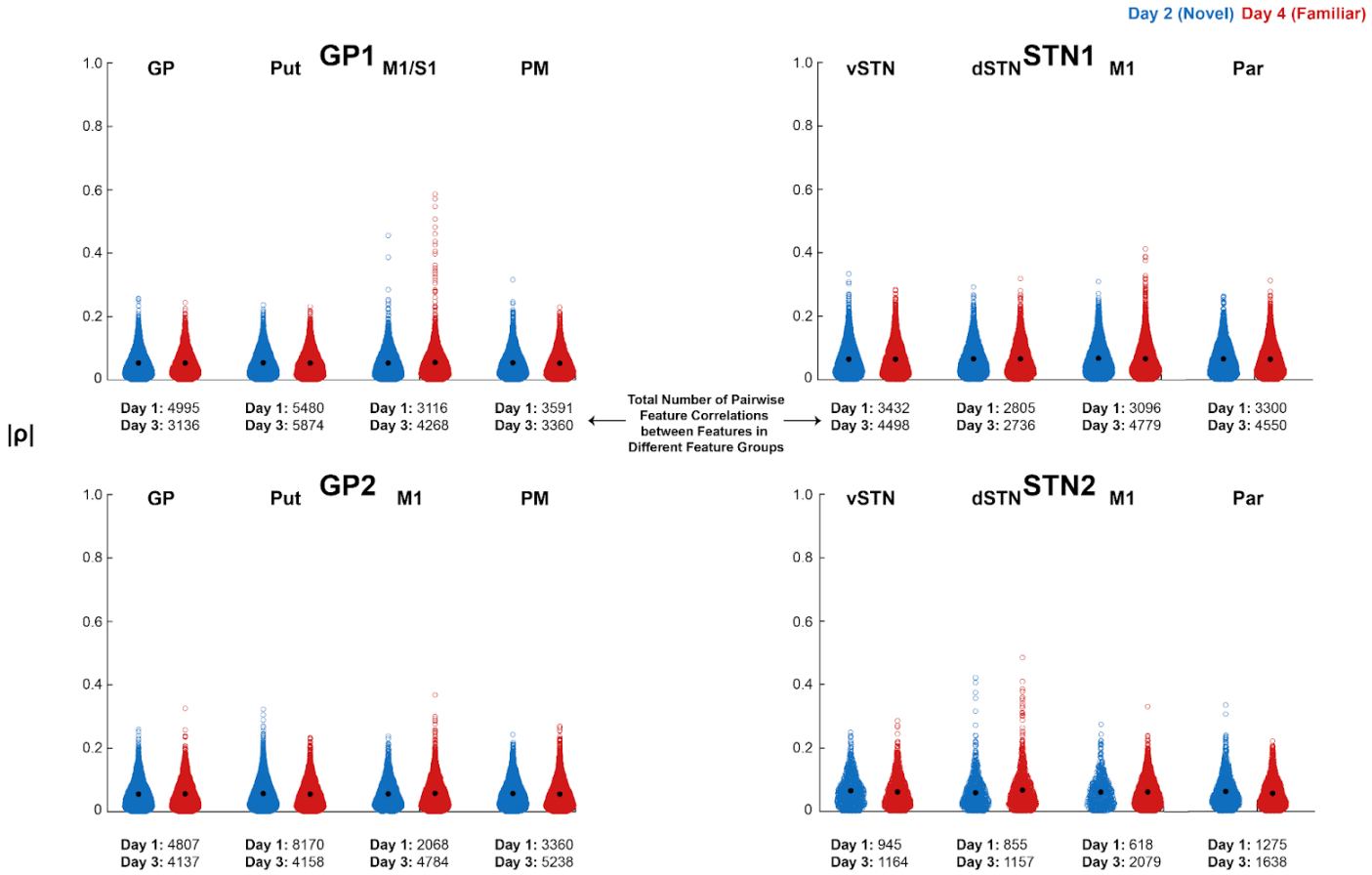

Figure 5–figure supplement 5. Correlations between features after grouping into 1) δ through β and 2) low γ through high γ. For each model, a swarm plot of all possible feature correlations between features in different groups. Features were grouped into δ through β (0.5–30 Hz) and low γ through high γ (30–250 Hz), with amplitude and phase features grouped together. Total number of feature correlations between features in different groups for a given model is shown below corresponding swarm plots.

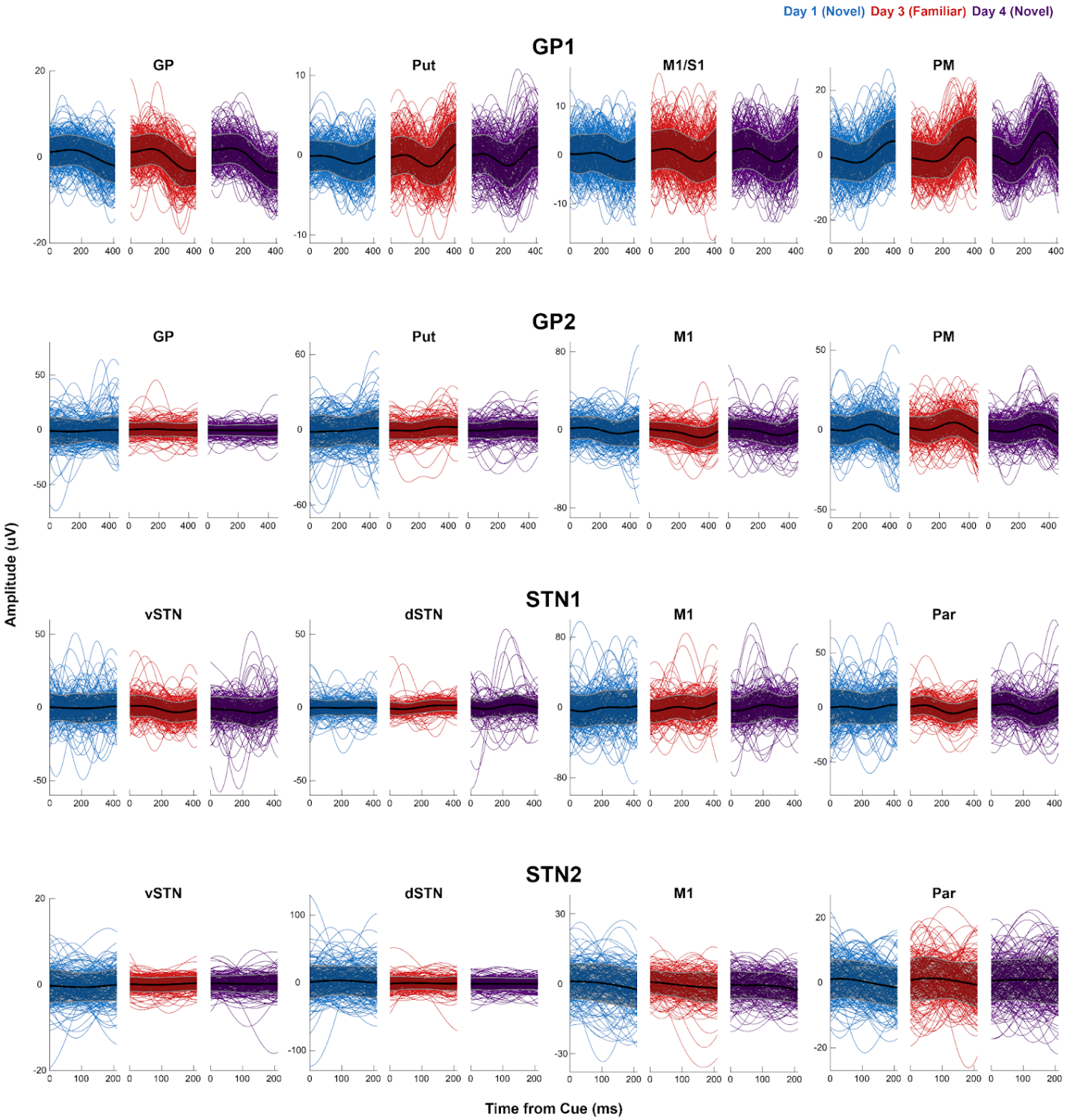

Figure 6–figure supplement 1. Single-trial δ time domain data. Data is aligned to cue onset and plotted as $\bar{x}\pm s$.

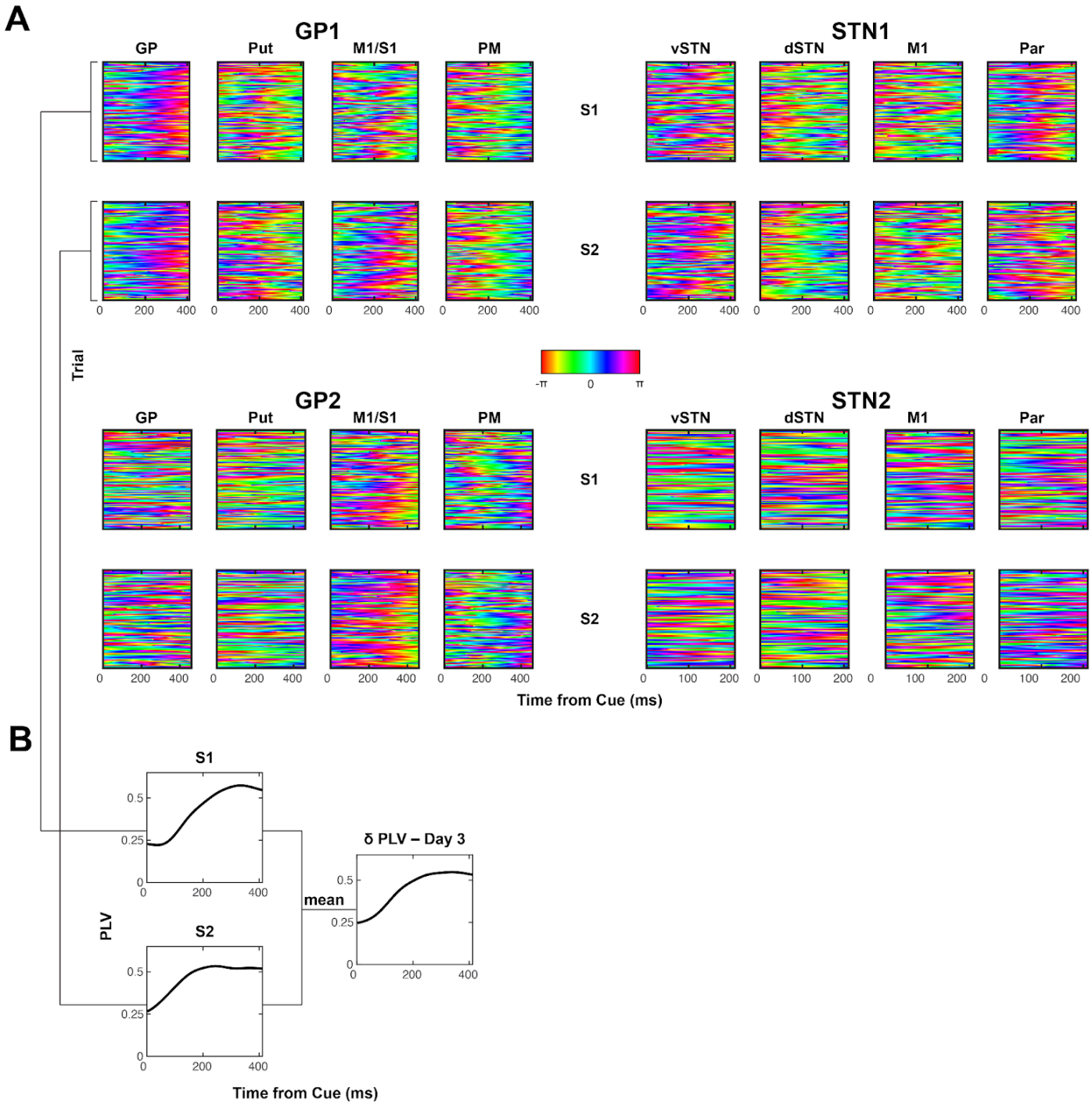

Figure 6–figure supplement 2. Day 3 single-trial δ phase. (**A**) δ phase data aligned to cue onset. (**B**) Example of phase locking value calculation. Phase locking value was first calculated within sequence and smoothed with a 150 ms-long Gaussian window. Resulting time series were averaged across the two sequences to compute the overall phase locking value for this brain region on this day.

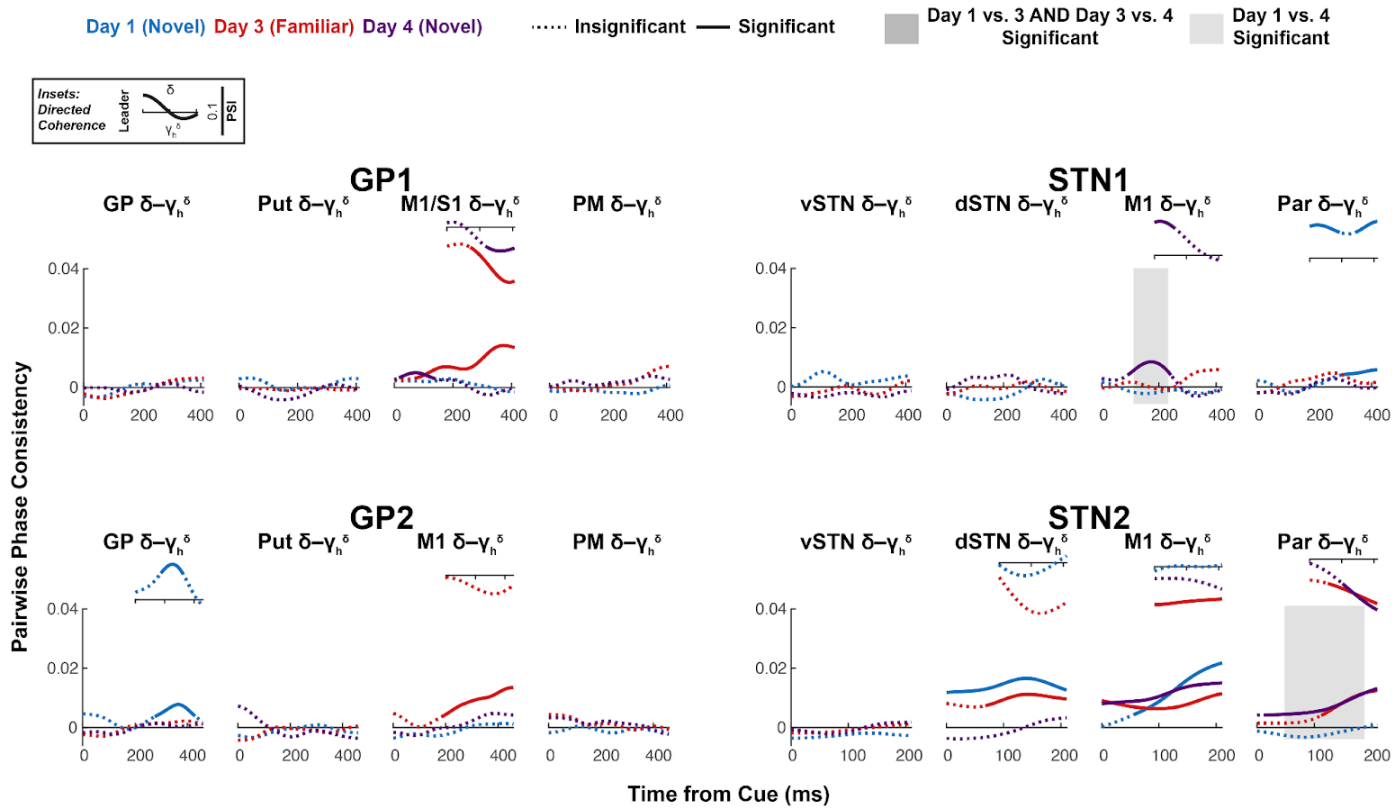

Figure 7–figure supplement 1. Intraregional δ-γ coupling. (Large plots) Pairwise phase consistency (PPC, undirected measure) was calculated between δ phase and the δ phase of the high γ amplitude envelope. Solid line indicates significant PPC (h_0=coherence is not higher than expected given the phase distribution, α=0.05, one-sided, cluster-based permutation with 10,000 resamples. Supplementary Data 7—2 *p*-Values). Shaded box indicates significant difference in PPC between days (α=0.05, two-sided, cluster-based permutation with 10,000 resamples. Supplementary Data 7—2 *p*-Values). (Insets) Phase slope index (PSI, directed measure) for significant PPC time series. Solid line indicates significant PSI (h_0=no channel leads, α=0.05, two-sided, cluster-based permutation with 10,000 resamples. Supplementary Data 7—2 *p*-Values).

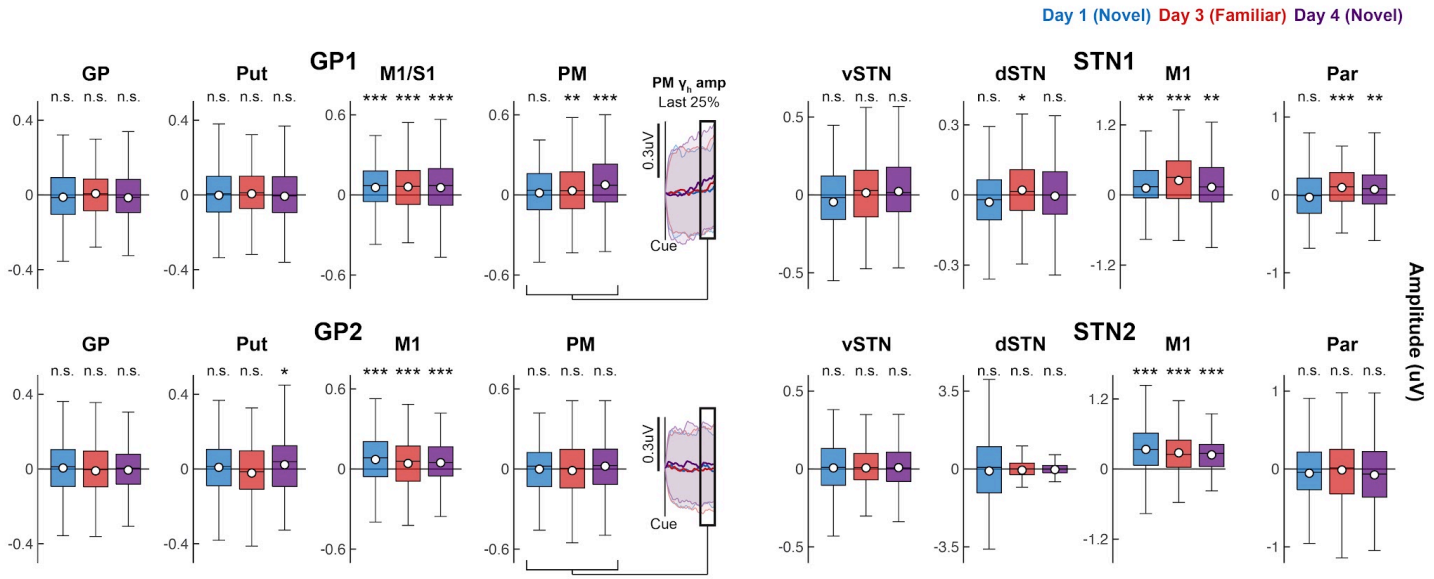

Figure 7–figure supplement 2. High γ amplitude distributions. (Box plots) Change in high γ amplitude from cue onset to the last 25% of the reaction time period, after linear interpolation of all RT period trials to the same length and smoothing of γ amplitude across time (α=0.05, one-sided, bootstrap estimation of $\bar{x}$ with 10,000 resamples. Supplementary Data 7—3 *p*-Values). White circle reflects mean; black horizontal line reflects median. Box edges correspond to 25th and 75th percentiles. Whiskers span entire data range excluding outliers. Outliers were computed as 1.5·*IQR* away from the upper or lower quartile and are not shown. (Insets) GP1 and GP2 trial average γ amplitude time series in premotor cortex, with black rectangle indicating the window over which γ amplitude is averaged for individual trials. Error bars indicate ±*s*. **p*<0.05, ***p*<0.01, ****p*<0.001.

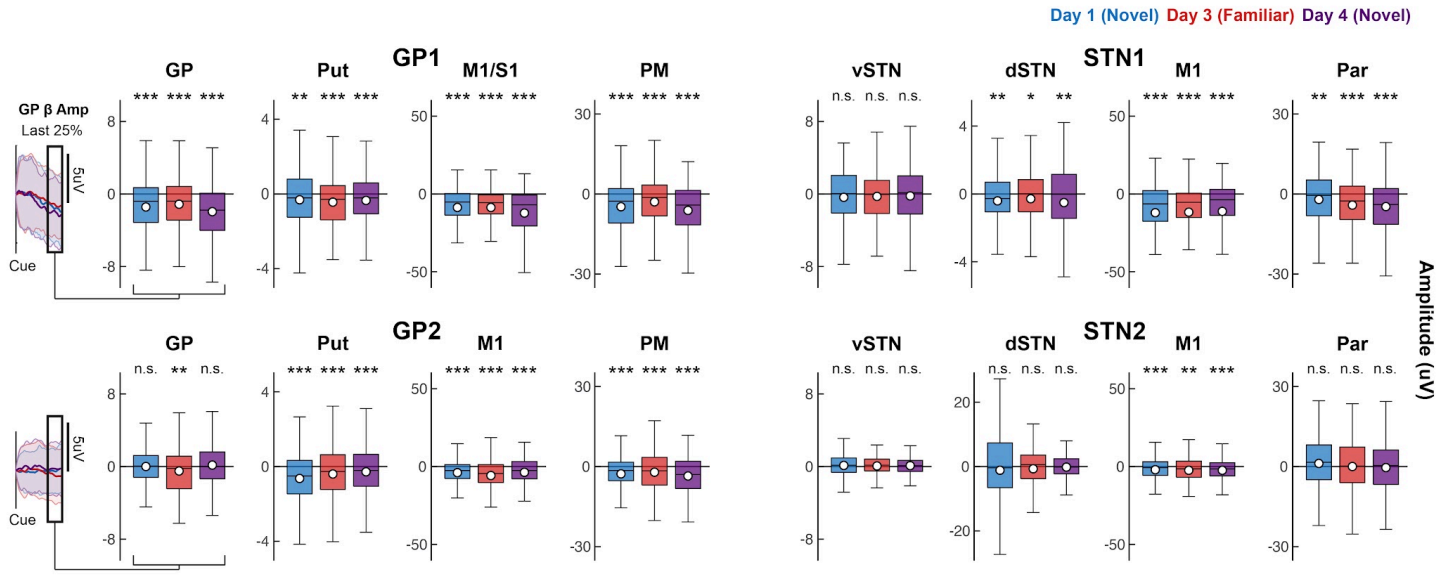

Figure 8–figure supplement 1. β amplitude distributions. (Box plots) Change in β amplitude from cue onset to the last 25% of the reaction time period, after linear interpolation of all RT period trials to the same length and smoothing of β amplitude across time (α=0.05, one-sided, bootstrap estimation of $\bar{x}$ with 10,000 resamples. Supplementary Data 7—3 *p*-Values). White circle reflects mean; black horizontal line reflects median. Box edges correspond to 25th and 75th percentiles. Whiskers span entire data range excluding outliers. Outliers were computed as 1.5·*IQR* away from the upper or lower quartile and are not shown. (Insets) GP1 and GP2 trial average β amplitude time series in pallidum, with black rectangle indicating the window over which β amplitude is averaged for individual trials. Error bars indicate ±*s*. **p*<0.05, ***p*<0.01, ****p*<0.001.

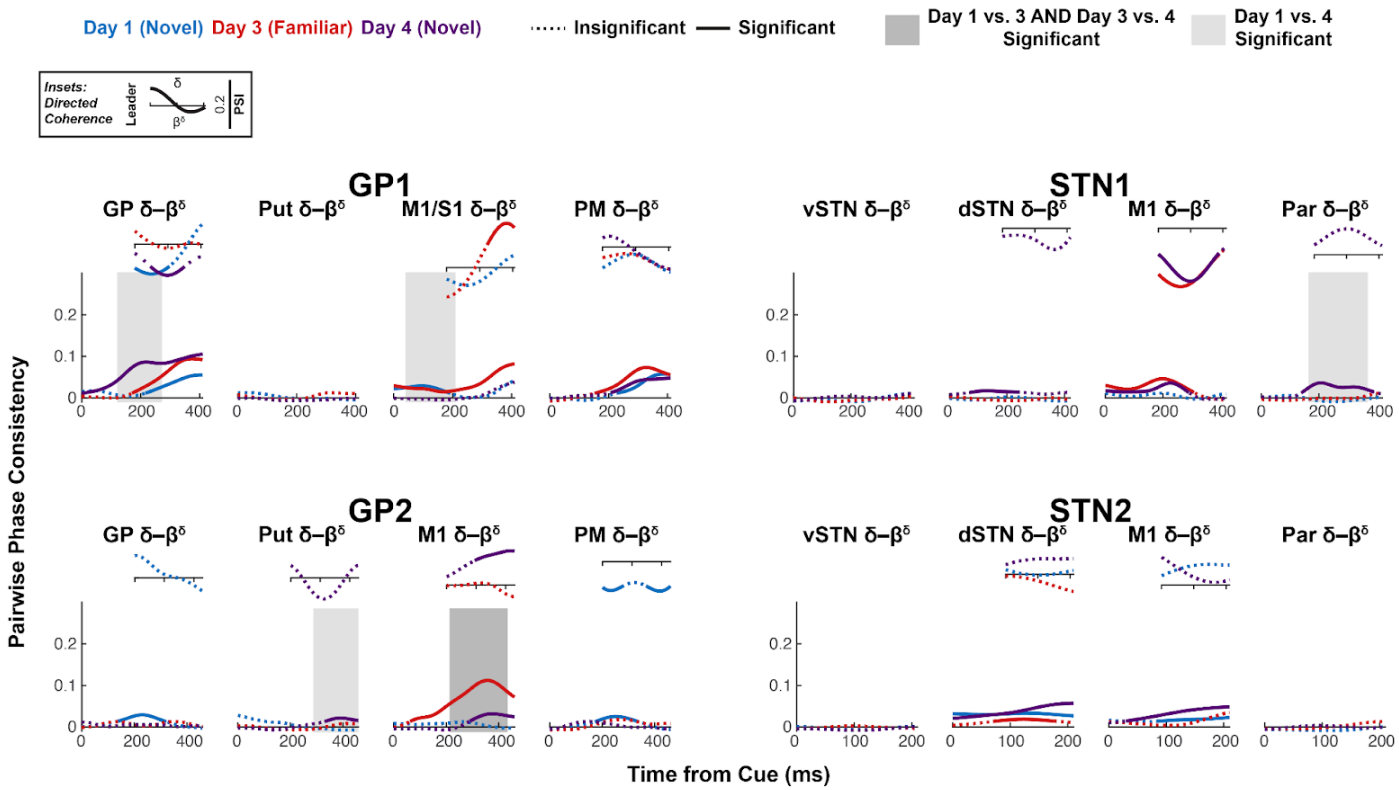

Figure 8–figure supplement 2. Intraregional δ-β coupling. (Large plots) Pairwise phase consistency (PPC, undirected measure) was calculated between δ phase and the δ phase of the β amplitude envelope. Solid line indicates significant PPC (h_0=coherence is not higher than that expected given the phase distribution, α=0.05, one-sided, cluster-based permutation with 10,000 resamples. Supplementary Data 8—4 *p*-Values). Shaded box indicates significant difference in PPC between days (α=0.05, two-sided, cluster-based permutation with 10,000 resamples. Supplementary Data 8—4 *p*-Values). (Insets) Phase slope index (PSI, directed measure) for significant PPC time series. Solid line indicates significant PSI (h_0=no channel leads, α=0.05, two-sided, cluster-based permutation with 10,000 resamples. Supplementary Data 8—4 *p*-Values).

TABLES

	Dominant Hand	Pre-Op MoCA	Pre-Op UPDRS ON Med	Pre-Op UPDRS OFF Med	% Change ON Med	Primary Symptoms
GP1	R	28	9	18	-50%	Hand tremor, bradykinesia, gait
GP2	R	27	17	31	-45%	Hand tremor, bradykinesia, gait
STN1	R	26	5	32	-84%	Hand tremor, bradykinesia
STN2	R	28	10	31	-68%	Hand tremor, bradykinesia

Table 1. Subject demographic and clinical information. MoCA, Montreal Cognitive Assessment; UPDRS, Unified Parkinson's Disease Rating Scale. *Given the small sample size, age and sex have been omitted to retain participant privacy.*

	Day				
	Familiarization	**1**	**2**	**3**	**4**
GP1	2-4-5-3-2 2-3-5-4-2	4-2-3-5-4 4-5-3-2-4	4-5-3-2-4 4-2-3-5-4	4-2-3-5-4 4-5-3-2-4	4-2-5-3-4 4-3-5-2-4
GP2	2-5-3-4-2 2-4-3-5-2	3-4-2-5-3 3-5-2-4-3	3-5-2-4-3 3-4-2-5-3	3-4-2-5-3 3-5-2-4-3	3-2-4-5-3 3-5-4-2-3
STN1	2-4-3-5-2 2-5-3-4-2	3-4-2-5-3 3-5-2-4-3	3-5-2-4-3 3-4-2-5-3	3-4-2-5-3 3-5-2-4-3	3-2-4-5-3 3-5-4-2-3
STN2	2-4-5-3-2 2-3-5-4-2	4-2-3-5-4 4-5-3-2-4	4-5-3-2-4 4-2-3-5-4	4-2-3-5-4 4-5-3-2-4	4-2-5-3-4 4-3-5-2-4

Table 2. Sequences. No sequences contained repeated adjacent elements, rising or falling triplets, or the thumb. All sequences paired for comparison within and across days started with the same first and last elements. Block order of S1 and S2 was switched on Day 2.

	Day	Postural Tremor	Kinetic Tremor	Finger Tapping	Hand Movements	Pronation/ Supination	Total	Prior Night's Sleep (hr)
GP1	**F**	1	1	2	2	1	7	7.75
	1	1	0	3	2	3	9	4
	2	1	1	3	2	2	9	8
	3	2	1	3	2	1	9	7
	4	1	1	2	2	2	8	7
GP2	**F**	1	2	2	3	1	9	7.5
	1	1	1	3	3	2	10	7
	2	1	2	2	2	1	8	8.25
	3	1	2	2	2	1	8	8
	4	2	2	2	2	1	9	8
STN1	**F**	1	0	2	1	2	6	7
	1	2	1	0	0	1	4	7.25
	2	1	0	0	1	0	2	8.5
	3	0	0	1	1	1	3	5.25
	4	1	0	0	0	1	2	8.75
STN2	**F**	1	0	2	2	1	6	6
	1	1	0	2	2	1	6	6.5
	2	0	1	2	2	1	6	9.5
	3	0	1	2	1	1	5	8
	4	0	1	2	2	1	6	8.5
		(R/task hand)	**Range: [0, 4]**	**0 = none, 4 = severe**				

Table 3. Supplementary data collection. Scores for the upper limb component of the UPDRS performed immediately after the typing task each day and the prior night's sleep duration, collected with a sleep journal. F, Familiarization.